

# **Pico-nano-micro-meso-kilo**

**August 7-9, 2018**

**Geosciences Research Program, Office of Basic Energy Sciences**

## **FOREWORD**

“Pico-nano-micro-meso-kilo” is the 23<sup>rd</sup> in a series of Geosciences Research Program Symposia dating from 1995. These symposia are meetings for principal investigators in the program and provide opportunities for our investigators to give presentations on their BES-supported research. It is hoped that this meeting will provide an environment conducive to building collaborations and identifying opportunities for new research directions. This year the PI meeting is Geosciences Program-wide, encompassing the entire breadth of research, and is organized in order of increasing scale (pico-nano-micro-meso-macro). We also have a guest presentation by Dr. David Yuen, of Columbia University and Wuhan University on Data Science. I would also like to thank Teresa Crockett and Diane Marceau (recently retired) of the Chemical Sciences, Geosciences, and Biosciences (CSGB) Division and Connie Lansdon of the Oak Ridge Institute for Science and Education (ORISE) for their contributions in organizing the technical and logistical aspects of this meeting.

Finally, I thank all the scientists whose vision and creativity in research and dedication and thoughtfulness in peer review have shaped the ongoing research mission of the Office of Basic Energy Sciences Geosciences Program.

Once again, we look forward to an outstanding series of presentations.

Jim Rustad

Geosciences Research Program

Office of Basic Energy Sciences

US Department of Energy

## Agenda

2018 Geosciences Program PI Meeting  
US Department of Energy  
Office of Basic Energy Sciences  
Chemical Sciences, Geosciences & Biosciences Division (CSGB)

### Monday Aug 6

4:00-6:00 pm Registration (if you miss this, you may register in the morning)

### Tuesday Aug 7

7:00 AM Breakfast

#### Introductions

7:55 AM Welcome, Jim Rustad, BES Geosciences Program Manager

8:00 AM BES/CSGB Update, Bruce Garrett, CSGB Division Director

8:30 AM BES Geosciences Program Update, Jim Rustad, BES Geosciences Program Manager

#### Session 1

9:00 AM *Advancing Understanding of Iron Oxide/Water Interfacial Reactivity Far From Equilibrium*

Kevin Rosso, Pacific Northwest National Laboratory

9:30 AM *Reactivity and Transformations of Minerals in Adsorbed H<sub>2</sub>O Films*

John Loring, Pacific Northwest National Laboratory

10:00 AM *Molecular dynamics simulations of water-saturated Na-smectite clay during one-dimensional consolidation*

Ian Bourg, Princeton University

10:30 AM Break

#### Session 2

10:45 AM *Complexity in Metal-Mineral Interactions*

Paul Fenter, Argonne National Laboratory

11:15 AM *Divalent Mn-promoted rapid transformation of layered to tunneled manganese oxide*

Mike Zhu, University of Wyoming

11:45 AM *Interfacial Geochemistry of Nanopores: Molecular Behavior in Subsurface Environments*

Anastasia Ilgen, Sandia National Laboratory

12:15 PM Working Lunch

### Session 3

- 1:30 PM *In-situ microanalysis of O & C isotope ratios in carbonate cements: Calcite revisited*  
John Valley, University of Wisconsin
- 2:00 PM *Nitrogen diffusion in minerals, with implications for terrestrial N cycling*  
Bruce Watson, Rensselaer Polytechnic Institute
- 2:30 PM *Spherulites, sprinkles, and concentric rings in coral skeletons*  
Pupa Gilbert, University of Wisconsin
- 3:15 PM *Poster Session I*
- 6:00 PM Working Dinner
- 7:30 PM Guest Lecture, David Yuen, Columbia University

### **Wednesday Aug 8**

- 7:00 AM Breakfast

### Session 4

- 8:00 AM *Seawater chemistry and carbonate mineral growth*  
Don DePaolo, Lawrence Berkeley National Laboratory
- 8:30 AM *Intramolecular isotope study of light hydrocarbons*  
Juske Horita, Texas Tech University
- 9:00 AM *Closing the gap between experimental thermodynamic measurements  
and theoretical energetic data obtained from computational efforts*  
Nadine Kabengi, Georgia State University

- 9:30 AM Break

### Session 5

- 9:45 AM *Atomic Structure, Defects, and Stacking of Clay Particles by Low-Dose, High Resolution  
(Cryo)-TEM*  
Michael Whittaker, Lawrence Berkeley National Laboratory
- 10:15 AM *Water under Ultra-confinement: Implications for Reactions, Transport, and Mineral  
Stability*  
Larry Anovitz, Oak Ridge National Laboratory

10:45 AM *Mineral precipitation in porous media: interplay between transport, nucleation, and growth.*

Vitalii Starchenko, Oak Ridge National Laboratory

11:15 AM John Vetrano, BES Materials Science & Engineering

11:30 AM Working Lunch and Strategic Planning

Session 6

1:00 PM *Multiphase flow in porous media: wetting, disorder, and pattern formation*

Ruben Juanes, Massachusetts Institute of Technology

1:30 PM *Genesis, storage, and leakage of shale gas*

Maria Mastalerz, University of Indiana

2:00 PM *Fracture Permeability Behavior at Subsurface Conditions*

Bill Carey/Hari Viswanathan, Los Alamos National Laboratory

2:30 PM Break

Session 7

2:45 PM *Applying machine learning to probe nonlinear elastic behavior in rock and fault-slip physics*

Paul Johnson, Los Alamos National Laboratory

3:15 PM *Investigating the Roughness and Advance Rate of the Weathering Interface in Shale: From Geochemistry to Geophysics*

Susan Brantley, Penn State University

4:00 PM *Poster Session II*

6:00 PM Working Dinner

**Thursday August 9**

7:00 PM Breakfast

Session 8

8:00 AM *3D Seismic Inverse Modeling: Applications to Full Waveform Imaging and Earthquake Source Moment Reconstruction*

Greg Newman, Lawrence Berkeley National Laboratory

8:30 AM *Calculating trajectories and imaging in a heterogeneous medium*

Don Vasco, Lawrence Berkeley National Laboratory

9:00 AM *Role of chemical-mechanical interaction in fracture size and spacing patterns*

Steve Laubach, University of Texas, Austin, Bureau of Economic Geology

9:30 AM Break

Session 9

9:45 AM *Properties and dynamics of the shallow crust*

Yehuda Ben-Zion, University of Southern California

10:15 AM *The spatial reach of induced seismicity*

Emily Brodsky, UC Santa Cruz

10:45 AM Adjourn

## Posters

Poster Session I (Tuesday, Aug 7, 3:15 PM)

1(baldwin) **An ultrahigh vacuum purification system for nitrogen and noble gas static mass spectrometry of crustal materials** S. L. Baldwin<sup>1</sup>, J. P. Das<sup>1\*</sup>, M.F. Schaller<sup>2</sup>, and E.B. Watson<sup>2</sup> <sup>1</sup>Syracuse University Noble Gas Isotopic Research Laboratory, Dept. of Earth Sciences, Syracuse, NY 13244; <sup>2</sup> Dept. of Earth & Environmental Sciences, Rensselaer Polytechnic Institute, Troy, NY 12180 \* now at EAG Laboratories, Syracuse, NY

1(bylaska) **Development of Novel First Principles Simulations for Reactions at Complex Geochemical Interfaces** Eric J. Bylaska, Pacific Northwest National Laboratory, Richland, WA

1(christensen) **Calcium, Carbon, and Oxygen Isotopic Fractionation Accompanying Carbonate Precipitation from High pH Waters at The Cedars, CA** John N. Christensen<sup>1</sup>, Donald J. DePaolo<sup>1,2</sup>, Mark S. Conrad<sup>1</sup>, James M. Watkins<sup>3</sup>, Marco Voltolini<sup>1</sup>, Shaun T. Brown<sup>1</sup> and Wenbo Yang<sup>4</sup> <sup>1</sup>Earth and Environmental Science Area, Energy Geosciences Division, Lawrence Berkeley National Laboratory, Berkeley, CA 94720. <sup>2</sup>Department of Earth and Planetary Science, University of California, Berkeley, CA 94720. <sup>3</sup>Department of Earth Sciences, University of Oregon, Eugene, OR 97403 <sup>4</sup>Department of Integrative Biology, University of California, Berkeley, CA 94720.

1(criscenti) **Molecular Modeling of Nanoparticle-Water Interactions: Adsorption and Aggregation** Louise J. Criscenti<sup>1</sup>, Tuan Ho<sup>1</sup>, Andrew S. Lee<sup>1</sup>, Jeffery A. Greathouse<sup>1</sup>, Kevin Leung<sup>2</sup>, and Yifeng Wang<sup>3</sup> <sup>1</sup>Geochemistry, <sup>2</sup>Nanostructure Physics, and <sup>3</sup>Nuclear Waste Disposal Research and Analysis Departments, Sandia National Laboratories, Albuquerque, NM 87185.

1(gilbert) **The Dynamics of Confined Aqueous Solutions** Baptiste Dzas<sup>1,2\*</sup>, Chris Colla<sup>3\*</sup>, Marzena Prus<sup>4</sup>, Karolina Kedra-Krolik<sup>4</sup>, Piotr Zarzycki<sup>3</sup>, Apple Li<sup>5</sup>, Ricardo H. R. Castro<sup>5</sup>, Ian C. Bourg<sup>1</sup> and Benjamin Gilbert<sup>3</sup> <sup>1</sup>. Department of Civil and Environmental Engineering, Princeton University <sup>2</sup>. Université de Poitiers, CNRS, UMR 7285 IC2MP, Equipe Hydrasa, Poitiers, France <sup>3</sup>. Energy Geoscience Division, Lawrence Berkeley National Laboratory, Berkeley CA <sup>4</sup>. Polish Academy of Science, Warsaw, Poland <sup>5</sup>. Peter A. Rock Thermochemistry Laboratory and NEAT ORU, University of California – Davis, Davis CA. \* equal co-authors

1(greathouse) **Modeling of Adsorption and Vibrational Properties at Hydroxylated Mineral Surfaces** Jeffery A. Greathouse<sup>1</sup>, Jacob A. Harvey<sup>1</sup>, Tuan A. Ho<sup>1</sup>, Kevin Leung<sup>2</sup>, Andrew S. Lee<sup>1</sup>, Louise J. Criscenti<sup>1</sup>, Rafael I. Gonzalez<sup>3</sup>, and Cliff T. Johnston<sup>4</sup> <sup>1</sup>Geochemistry and <sup>2</sup>Nanostructure Physics Departments, Sandia National Laboratories, Albuquerque, NM 87185; <sup>3</sup>Universidad Mayor, Santiago 8580745, Chile; <sup>4</sup>Crop, Soil and Environmental Sciences, Purdue University, West Lafayette, IN 47907

1(hochella) **Formation Mechanisms, Crystal Structure, and Interfacial Reactivity of (Mixed) Metal Sulfide Nanoparticles Produced via Biological versus Abiotic Systems** Jie Xu, Muammar Mansor, Mitsu Murayama, and Michael Hochella, Virginia Tech, Blacksburg, VA

1(lee) **Effect of anions on the formation and uptake of Zr nanoparticles at the muscovite (001) surface** Ke Yuan,<sup>1</sup> Jacquelyn N. Bracco,<sup>1</sup> Moritz Schmidt,<sup>2</sup> L. Soderholm,<sup>1</sup> Paul Fenter,<sup>1</sup> and Sang Soo Lee<sup>1</sup> <sup>1</sup> Chemical Sciences and Engineering Division, Argonne National Laboratory. 9700 South Cass Avenue,

Argonne, IL 60439; <sup>2</sup>Helmholtz-Zentrum Dresden-Rossendorf, Institute of Resource Ecology, Dresden, Germany

1(pester) **Kinetics of D/H isotope fractionation between molecular hydrogen and water** Nicholas J. Pester <sup>a,b,\*</sup>, Mark E. Conrad <sup>a</sup>, Kevin G. Knauss <sup>a</sup>, Donald J. DePaolo <sup>a,b</sup> <sup>a</sup>Energy Geosciences Division, Lawrence Berkeley National Lab., Berkeley, CA 94720, USA <sup>b</sup>Dept. of Earth and Planetary Science, University of California, Berkeley, CA 94720, USA \*corresponding email: [njpester@lbl.gov](mailto:njpester@lbl.gov)

1(prange) **Understanding Photoexcited Charge Transport Reactivity at Geochemical Nanoparticle Interfaces**, *Micah P. Prange and Kevin M. Rosso*, Physical Sciences Division, Pacific Northwest National Laboratory, Richland, Washington 99352

1(schaller) **A potential new proxy for paleo-atmospheric pO<sub>2</sub> from soil carbonate-hosted fluid inclusions**, Morgan F. Schaller<sup>1</sup>, Elizabeth A. Pettitt<sup>1</sup>, Todd K. Knobbe<sup>1</sup>, Daniel O. Breecker<sup>2</sup>, E. Bruce Watson<sup>1</sup> <sup>1</sup>Earth and Environmental Sciences, Rensselaer Polytechnic Institute, Troy, NY <sup>2</sup>Jackson School of Geosciences, University of Texas at Austin, Austin, TX

Poster Session II (Wed, Aug 8, 4:00 PM)

2(buscarnera) **Simulating the feedbacks between grain-scale crack growth and delayed comminution in fluid-saturated granular solids** G. Buscarnera, Northwestern University, Evanston, IL

2(goebel) **The spatial footprint of injection wells in a global compilation of induced earthquake sequences** Thomas Goebel and Emily Brodsky, University of California, Santa Cruz, Santa Cruz, CA

2(ladd) **Dissolution at the pore scale: comparing simulations and experiments** Anthony Ladd, Vitaliy Starchenko, Filip Dutka, and Piotr Szymczak University of Florida

2(martinez-lorenzo) **Fusing Thermoacoustic, Electromagnetic and Acoustic/Seismic Wave Fields for Subsurface Characterization and Imaging of Flow Transport**. Chang Liu<sup>1</sup>, Richard Obermeier<sup>2</sup>, Ashkan Ghanbarzadeh Dagheyan<sup>1</sup>, Juan Heredia Juesas<sup>1,2</sup>, Ali Molaei<sup>2</sup>, and Prof. Jose A. Martinez Lorenzo<sup>1,2</sup>, <sup>1</sup>Department of Mechanical and Industrial Engineering, <sup>2</sup>Department of Electrical and Computer Engineering, Northeastern University, Boston, MA.

2(pride) **New rules of multiphase flow as constrained by lab measurements and simulations** Steve Pride, Lawrence Berkeley National Laboratory, Berkeley, CA

2(pyrak-nolte) **Swarm Transport in Fractures and Porous Media**, Laura J. Pyrak-Nolte<sup>1,2,3</sup>, Chven Mitchell<sup>2</sup>, Ludwig Nitsche<sup>4</sup>, <sup>1</sup>Department of Physics and Astronomy, <sup>2</sup>Department of Earth, Atmospheric and Planetary Sciences, <sup>3</sup>Lyles School of Civil Engineering, Purdue University, West Lafayette, Indiana; <sup>4</sup>Department of Chemical Engineering, The University of Illinois at Chicago, Chicago, IL.

2(shaw) **Distributary Channel Networks modeled through Non-linear Viscous Fingering** John B. Shaw, Wun-Tao Ke, Robert Mahon, Chris Cathcart University of Arkansas

2(shokouhi) **Coupled assessment of seismic, hydraulic, and frictional properties of fractured rock to illuminate fundamental processes governing energy production and waste storage**, Parisa Shokouhi<sup>1</sup>, Jacques Rivière<sup>1</sup>, Derek Elsworth<sup>2</sup> and Chris Marone<sup>3</sup>, <sup>1</sup> Engineering Science and Mechanics, <sup>2</sup>Dept. of Energy and Mineral Engineering and Energy Institute, <sup>3</sup>Dept. of Geosciences, The Pennsylvania State University

2(tournassat) **Shales and geological waste repositories: from microstructure description to macro-scale properties** Christophe Tournassat<sup>1,2,3</sup>, Stéphane Gaboreau<sup>2</sup>, Carl I. Steefel<sup>1</sup> <sup>1</sup> Energy Geoscience Division, Lawrence Berkeley National Laboratory, Berkeley, CA 94720, USA <sup>2</sup> BRGM, Orléans, 45060, France <sup>3</sup> Univ. Orléans, UMR 7327 CNRS-BRGM-ISTO, 45071 Orléans, France

## Water under Ultra-confinement: Implications for Reactions, Transport, and Mineral Stability

Lawrence M. Anovitz

<sup>1</sup>*Chemical Sciences Division, Oak Ridge National Laboratory, Oak Ridge, Tennessee 37831, USA*

In order to predict the effects of pore-confinement on reactivity, we must understand how water properties change relative to open solutions. The most extreme such effects will be observed for molecularly-confined (i.e., “ultraconfined”) water in nanoscale channel or cage-like mineral structures. Water in such materials is confined in environments not much larger than the water molecule itself, and thus presents an end-member example of confinement effects. While such mineralogical confinement may be fairly specific to the mineral structure, they provide geometrically and chemically well-defined environments in which specific effects can be addressed. In addition, as pressures increase in geological environments grain boundaries between minerals tend to close, becoming similar-scale environments. Thus, mineral ultraconfinement studies provide well-constrained examples of a state likely very common in nature.

To understand this state, we have performed computational and neutron scattering studies of ultraconfined water in subnanometer channels in the minerals beryl, cordierite, hemimorphite, diopside, and mordenite (Anovitz et al., 2013; Kolesnikov et al., 2014, 2016, 2018; Podlesnyak et al., 2016; Prisk et al, 2018). These vary in confining geometry and water bond structure, and confinement affects the thermodynamic and thermophysical of the water and even magnetic properties of the solid. In beryl INS showed no hydrogen bonds acting on water molecule at low temperatures, and a strongly anisotropic potential, steep along the channels and soft perpendicular to it. QENS data revealed gradual freezing out of the water molecule when the scattering momentum transfer was parallel to the channels, but not perpendicular to the channels. At 4.3 K the average kinetic energy of the water molecules was ~30% less than in bulk liquid water and ice, but DINS and INS at higher temperatures showed a significant increase in  $E_k$  of the protons and progressive hydrogen bonding with the beryl cage, consistent with our dielectric spectroscopy results. In addition, a “quantum tunneling state” was found for these water molecules characterized by extended proton and electron delocalization, the first ever shown for an asymmetric molecule.

By contrast, in hemimorphite (Figure 1), water molecules form a planar hydrogen bond network with hydroxyl groups that undergo a continuous orientational phase transition. The incoherent dynamic structure factor reveals two thermally activated relaxation processes, a faster one on the subpicosecond time scale and a slower one on the 10-100 ps time scale, between 70-130 K. The slow process is an in-plane reorientation involving breaking hydrogen bonds analogous to rotational diffusion of water molecules in the bulk liquid. The fast process is a localized water motion that has no apparent analogs to previously known bulk or confined water phases.

The processes described above directly influence thermochemical properties such as the heat capacity of ultraconfined water as a function of both the surrounding chemistry and temperature and may involve quantum effects under the right conditions. Future work will consider how the diffusion and reactivity of water in other tightly-confined geometries in rocks, such as in grain boundaries, are affected. This may represent a hitherto unappreciated driver of reactivity and limitation to calculations based on bulk water. Once water becomes confined to nanoscale grain boundaries it is unlikely that its

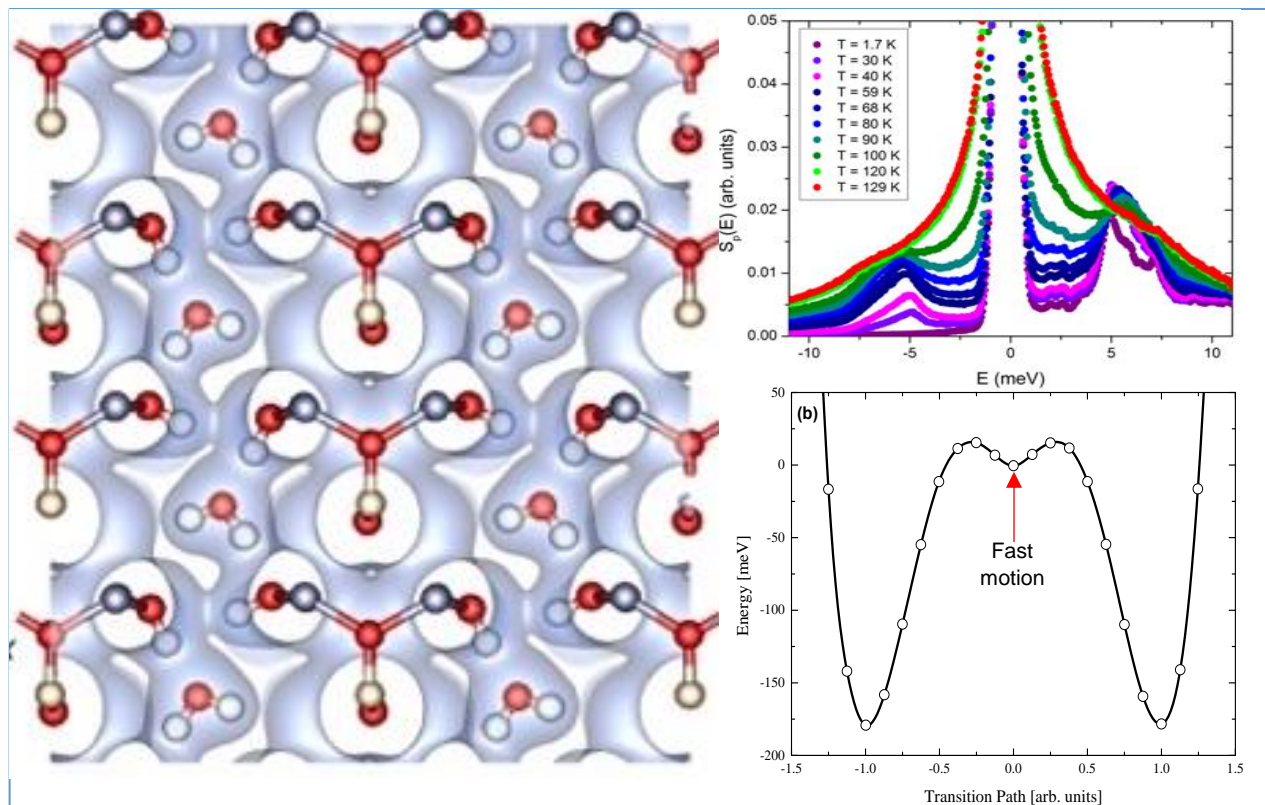


Figure 2. Left) DFT structure and isosurface of electronic charge density in hemimorphite showing alternating H<sub>2</sub>O positions. Looking down y, z vertical, x horizontal. (blue – Zn, Yellow – Si, Red – O, White - H. Upper right) CNCS data showing very broad (fast) QENS signal. Lower right) Orientational potential barrier of H<sub>2</sub>O molecule showing origin of the fast motion.

properties match those of the bulk material, thus affecting the stability of the surrounding mineral phases.

Anovitz, L. M., E. Mamontov, P. ben Ishai, and A. I. Kolesnikov, 2013, Anisotropic dynamics of water ultraconfined in macroscopically oriented channels of single-crystal beryl: A multifrequency analysis: *Physical Review E*, 88, 052306.

Kolesnikov, A. I., G. F. Reiter, T. R. Prisk, M. Krzystyniak, G. Romanelli, D. J. Wesolowski, and L. M. Anovitz, 2018, Inelastic and deep inelastic neutron spectroscopy of water molecules under ultra-confinement: *Journal of Physics: Conference Series*, 1055, 012002.

Kolesnikov, A., L. M. Anovitz, E. Mamontov, A. Podlesnyak, and G. Ehlers, 2014, Strong Anisotropic Dynamics of Ultra-Confined Water: *The Journal of Physical Chemistry B*, 118, 13414-13419.

Kolesnikov, A. I., G. F. Reiter, N. Choudhury, T. R. Prisk, E. Mamontov, A. Podlesnyak, G. Ehlers, A. G. Seel, D. J. Wesolowski, and L. M. Anovitz, 2016, Quantum Tunneling of Water in Beryl: A New State of the Water Molecule: *Phys. Rev. Lett.*, 116, 167802

Podlesnyak, A., L. M. Anovitz, A. I. Kolesnikov, M. Matsuda, T. R. Prisk, S. Toth, and G. Ehlers, 2016, Coupled antiferromagnetic spin-1/2 chains in green diopside Cu<sub>6</sub>[Si<sub>6</sub>O<sub>18</sub>] · 6H<sub>2</sub>O: *Physical Review B*, v. 93, p. 064426.

Prisk, T. R., C. Hoffmann, A. I. Kolesnikov, E. Mamontov, A. A. Podlesnyak, X. Wang, P. R. C. Kent, and L. M. Anovitz, 2018, Fast Rotational Diffusion of Water Molecules in a 2D Hydrogen Bond Network at Cryogenic Temperatures.: *Phys Rev Lett*, v. 120, no. 19, p. 196001.

## An ultrahigh vacuum purification system for nitrogen and noble gas static mass spectrometry of crustal materials

S. L. Baldwin<sup>1</sup>, J. P. Das<sup>1\*</sup>, M.F. Schaller<sup>2</sup>, and E.B. Watson<sup>2</sup>

<sup>1</sup>Syracuse University Noble Gas Isotopic Research Laboratory, Dept. of Earth Sciences, Syracuse, NY 13244; <sup>2</sup> Dept. of Earth & Environmental Sciences, Rensselaer Polytechnic Institute, Troy, NY 12180

\* now at EAG Laboratories, Syracuse, NY

The concentrations of C and N in rock-forming minerals as a function of depth in the crust is largely unknown from measurements on natural samples. This project aims to investigate N and Ar concentrations, and isotopic compositions, of sample gas extracted from chert and silicate minerals. The project is part of a larger collaborative effort to determine the amounts and locations of C and N stored in the crust, and whether and how crustal reservoirs might exchange these elements with the surface over geologic time. To enable coupled N and Ar analyses on sample gas extracted from crustal materials by static gas source mass spectrometry a dedicated N purification system was designed, fabricated from a 3D prototype, and attached to an existing ultrahigh vacuum (UHV) extraction line in the Syracuse University Noble Gas Isotopic Research Laboratory (SUNGIRL). Design modifications aimed to allow for maximum flexibility in terms of degassing samples via either furnace step heating, CO<sub>2</sub> laser heating, UV laser ablation, or crushing under UHV conditions, combined with purification prior to static gas source mass spectrometry. The new glass line is isolated from the all metal extraction line using two manual valves, and consists of a CuO finger, a cold finger and a pressure gauge. The following tasks, relevant to gas extraction, purification and mass spectrometric analyses, were completed during this reporting period. *Gas extraction:* A Cu plchette was designed and fabricated for extraction of N standards encapsulated in capillary tubes using a CO<sub>2</sub> laser. A sample crusher attachment to the UHV extraction line will be incorporated for applications involving extraction of gases from sample vesicles. *Nitrogen purification vacuum line.* A modified glass line was installed that incorporated a new MKS-390 modular vacuum gauge, to measure pressures in the range of 10<sup>3</sup> to 10<sup>-9</sup> torr (i.e. from atmosphere to UHV). A LabVIEW<sup>®</sup> program was written to control the MKS gauge as well as to monitor pressures in the dedicated N purification system. A cylindrical heater for the CuO finger was designed, constructed, and tested. CuO wires packed in Pt foil in a glass finger are heated to oxidize CO and convert to CO<sub>2</sub> which can be trapped using liquid N on a cold finger in order to avoid <sup>12</sup>C<sup>16</sup>O interferences with <sup>14</sup>N<sup>14</sup>N measurements. Bakeout hoods for the entire UHV extraction line, were modified to accommodate the dedicated N purification line and MKS gauge. Bake-out of the full extraction line table was performed to achieve pressures ~2 x 10<sup>-9</sup> torr. *Mass spectrometer modifications:* A requirement for upgrading software that runs the 5400 mass spectrometer included installation of a new Ortec ion counter. A new potentiometer, used to modify the trap current, was installed and calibrated to enable optimization of tuning parameters for nitrogen isotopic analyses. *Software development:* LabVIEW<sup>®</sup> software was written to control the MKS pressure gauge used to monitor pressures in the glass N purification line. An alpha version of LabVIEW<sup>®</sup> software (NGS54) to control the Micromass 5400 mass spectrometer was written and tested. While a beta version of NGS54 is further developed, we retained the capability of using the original (ng290) software (written in Modula 2) together with the original Micromass ion counter, during further development of analytical protocols. The noble gas and nitrogen isotopic data to be collected will be used to assess the capacity of crustal materials to capture, store, and retain a record of ancient atmospheric gases.

## **Properties and Dynamics of the Shallow Crust**

Yehuda Ben-Zion

Department of Earth Sciences, University of Southern California, Los Angeles, CA, 90089-0740, USA

### **Abstract**

I review multi-scale/signal seismological results on imaging the top few hundred meters of the crust, monitoring temporal changes of seismic velocities, and efforts to detect and classify different sources of weak motion contained in continuous seismic waveforms. The studies are based on seismic waveforms recorded by regional stations, dense arrays and borehole sensors. The results indicate that the shallow sub-surface material has extreme seismic properties (very low  $V_p$ ,  $V_s$ ,  $Q$  values, very high  $V_p/V_s$  ratios) that make it highly susceptible to nonlinear behavior and temporal changes. Large earthquakes produce rock damage (reduction of  $V_p$ ,  $V_s$ ,  $Q$ ) in broad shallow regions around the rupture zones. The co-seismic changes in the top few hundred meters are very large (>30-50% velocity reduction) and are followed by  $\log(t)$  recovery. Continuous waveforms consist mostly (~99%) of ground motion generated by wind-related events, air-traffic events and other natural & anthropogenic noise sources. Efforts to detect small seismic events (earthquakes, tremor) with unsupervised techniques and no validation are likely to produce many false detections.

\*The research was done in collaboration with F. Vernon, G. Hillers, D. Zigone, H. Meng, C. Johnson, L. Qin, P. Roux, M. Campillo, A. Mordret, F. Bonilla, Z. Peng & others

---

## **Molecular dynamics simulations of water-saturated Na-smectite clay during one-dimensional consolidation**

Thomas Underwood & [Ian C. Bourg](#)

*Department of Civil and Environmental Engineering and Princeton Environmental Institute, Princeton University*

Fine-grained sedimentary rocks such as shale or mudstone are ubiquitous in sedimentary basins and play important roles as caprocks, host rocks, or source rocks in many energy technologies including carbon capture and storage, nuclear waste storage, and hydrocarbon extraction. Accurate predictive models of the properties of these rocks remain elusive, however, because of the significant experimental challenges posed by their low mechanical strength, ultra-low permeability, and sensitivity to geochemical and geomechanical alteration. An even greater challenge is that the properties of these rocks are controlled by nanoscale interactions between water, ions, and clay particles that give rise to strong couplings between chemistry, mechanics, and hydrology. Here, we present an attempt to gain insight into these nanoscale interactions and couplings by developing an atomistic-level model of the microstructure of water-saturated clay during one-dimensional consolidation. Specifically, we carried out molecular dynamics (MD) simulations of aqueous suspensions of tens of Na-smectite clay nanoparticles (> 2 million atoms). We simulated the one-dimensional consolidations of these hydrated clay systems and characterized their microstructure, aqueous chemistry, and transport properties as a function of solid-water ratio. Our results shed new light into the manner in which the microstructure of nanoparticle assemblages influences water and solute diffusion, permeability, electrical conductivity, and dielectric properties in microporous clay.

## Investigating the Roughness and Advance Rate of the Weathering Interface in Shale: From Geochemistry to Geophysics

S.L. Brantley<sup>1,2</sup>, X. Gu<sup>2</sup>, A. Nyblade<sup>2</sup>, M. Lebedeva<sup>1</sup>, G. Mavko<sup>3,1</sup> Pennsylvania State University, Earth and Environmental Systems Institute, Univ. Pk PA 16802<sup>2</sup> Pennsylvania State University, Dept. of Geosciences, Univ. Pk PA 16802<sup>3</sup> Stanford University, Dept. of Geophysics, Stanford, CA 94305

As shales are exhumed and approach the earth's surface, they respond both chemically and physically. We are investigating these processes as they occur by focusing on several shales weathering in three watersheds experiencing different erosion rates (from high to low erosion rate: Fushan Taiwan; Eel River, CA; Shale Hills, PA). The three shales are roughly similar in composition and mineralogy. The erosion rate can be conceptualized as the rate that the shale is brought up through the weathering zone: it determines the residence time of shale particles as they move upward and are removed by erosion at the land surface. Most of our work focusses on the Rose Hill shale weathering in central Pennsylvania.

The deepest chemical reaction in all three shales is dissolution of carbonate minerals (calcite, ankerite), and oxidative dissolution of pyrite [Gu, 2017]. The oxidation of pyrite first results in formation of ferrihydrite *in situ*, then this transforms at shallower depths to goethite or hematite, which eventually re-crystallizes into goethite in fractures or pores at the shallowest depths. Under the ridges of the weathering shale in CA and PA, pyrite oxidizes near the water table at tens of meters depth. The next reaction that occurs is the transformation of chlorite to vermiculite, followed by illite dissolution. In both cases, the extent of these clay reactions decrease with increasing erosion rate.

As weathering proceeds, the reactions create porosity. In the Pennsylvania shale, most of the porosity is created from the reaction of chlorite. In contrast, in the two fast-eroding shales, only a small amount of the porosity that grows is due to chemical reaction: at least 40% of the secondary porosity is due to growth of microfractures in the weathering rock. The growth of microfractures in the fast-eroding shales is likely caused by the higher quartz + plagioclase content of those two shales as compared to the slow-eroding shale or the inability of the faster-eroding shales to heal microfractures because of the short residence time in the weathering and fracturing zone.

We plan to put these observations together with geophysical observations for the slow-eroding watershed using downhole logs of gamma ray, density, neutron porosity, optical viewer, and sonic log. Logs show that most of the fracturing in the shale occurs above the water table; however, one borehole log reveals the existence of at least two fractured layers (21.9-22.3 mbls and 24.7-25.8 mbls) that are present below the fluctuations of the water table (roughly from 18.1 to 19.5 mbls). These layers have lower density, higher porosity, and higher fracture density. The geochemical analysis further confirmed the weathering signature of these two more fractured layers: pyrite is observed to be depleted as determined by carbon/sulfur analysis and chlorite has been vermiculitized, as determined by X-ray diffraction and scanning electron microscopy. Thus it is clear that although most pyrite oxidizes above the water table under the ridges, the first oxidation occurs along deeper fractures that must bring oxygen-containing water to depth. Therefore, the reaction front for pyrite under the watershed roughly mimics the shape of the land surface but with lower relief, but also extends to much greater depths along some fractures.

To investigate the 3D nature of the reaction fronts and fracture patterns, we are developing a 3D seismic image of the shallow subsurface for the Pennsylvania shale. We have completed a 3D refraction seismic experiment in the watershed using 4200 geophones deployed at a 2 m spacing across about 1/3 of the watershed encompassing the boreholes with geophysical logs. Forty scientists and volunteers from 8 universities helped collect the data over seven days. Early results show excellent data collection that will reveal the 3D fine scale structure in the subsurface of the weathering shale.

Gu, X. (2017), Characterizing Structure and Geochemistry of Shale Pores by Neutron Scattering, Ph.D. Dissertation, Pennsylvania State University.

## Simulating the feedbacks between grain-scale crack growth and delayed comminution in fluid-saturated granular solids

G. Buscarnera<sup>1</sup> *Northwestern University*

Granular materials play a key role in disparate fields of technology and geophysics. A challenge concerning the mechanics of particulate geophysical solids is their response to the pressures acting in the lithosphere. At high pressure, the micromechanics of granular matter is controlled by particle strength, as well as by distributed grain damage. This project aims to elucidate the processes that control the long-term mechanics of fluid-saturated granular rocks, which is pivotal to explain the patterns of crushing, compaction and faulting in the lithosphere. For this purpose, the project aims to formulate and validate hypotheses about the interplay between fluid-assisted particle fracture, macroscopic comminution, and attributes such as grain size, shape, sorting, and mineralogy.

During the first phase of the project a continuum theory to quantify delayed compaction in fluid-saturated granular solids was formulated. Macroscopic inelastic strains were hypothesized to result from physico-chemical processes at the micro-cracks of individual grains, thus implying that crack growth at particle scale is one of the governing mechanism for the time-dependent, water-sensitive compression of granular systems. First, the fracture of particles in surface-reactive environments was studied. The analysis showed that the Gibbs adsorption isotherm is a central element to link the reduction of the fracture toughness of grain minerals to the increase of vapor concentration. This methodology was extended to particle assemblies immersed in wet environments, for which solid-fluid interfaces were treated as a separate phase. It was shown that this choice incorporates an adsorption isotherm into a continuum model, thus replicating the reduction of the yield strength as a function of relative humidity. The results show that the new framework facilitates the use of grain-scale properties in continuum simulations, thus providing a versatile platform to study a range of multi-scale, multi-physical couplings. Current activities are focused on the formulation of multi-scale computational tools, as well as on laboratory experiments verifying the hypotheses of the model directly at the grain-scale via microscopic imaging based on X-ray microtomography.

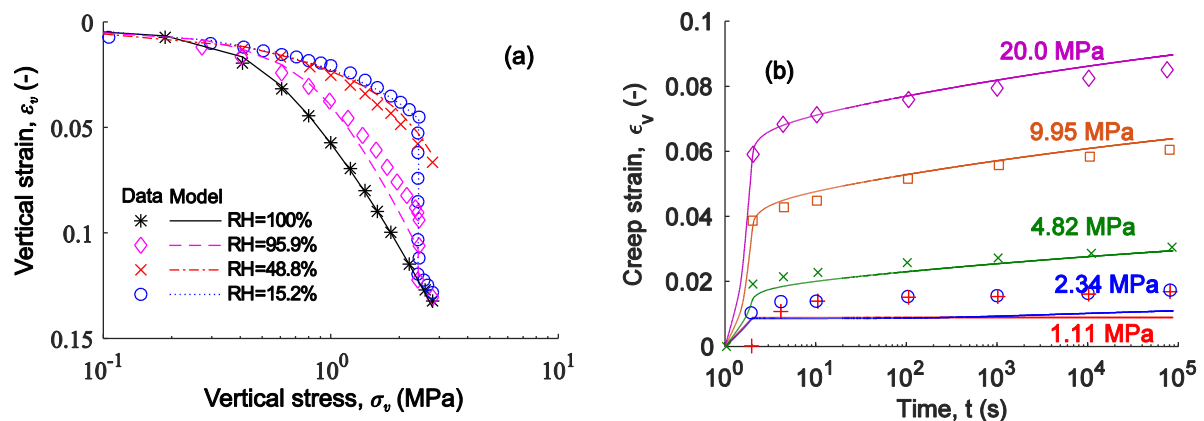


Fig. 1: (a) Confined compression followed by saturation in an unsaturated crushable granular material. The example illustrates the ability of the proposed theory to capture the increase in skeleton stiffness resulting from a decrease of relative humidity, as well as its ability to replicate the compaction processes induced by saturation. (b) Data vs. model predictions for creep tests conducted on sand after confined compression. The example illustrates the ability of the proposed constitutive law to replicate the pressure-dependence of compaction creep in granular materials subjected to high compressive stresses. It is shown that creep tends to be negligible below a threshold stress and grows as soon as delayed intra-grain fracture is triggered by larger stresses.

#### Recent Publications

Zhang, Y.D., Buscarnera, G. (2018). Breakage mechanics for granular materials in surface-reactive environments. *Journal of the Mechanics and Physics of Solids*, 112, 89-108.

Shahin, G., Cil, M., Buscarnera, G. (2018). Assessment of statistical homogeneity in chemically treated granular materials. *Géotechnique Letters*, 8(1), 1-21.

Marinelli, F., Buscarnera, G. (2018). A Generalized Backward Euler algorithm for the numerical integration of a viscous breakage model. To appear in *International Journal for Numerical and Analytical Methods in Geomechanics*.

## Development of Novel First Principles Simulations for Reactions at Complex Geochemical Interfaces

Dr. Eric J. Bylaska (PNNL)

The interpretation and prediction of mineral interactions with reservoir fluids is limited by the chemical complexity of the interface and the lack of experimental probes that definitively probe this region. The parameter free first-principle based simulation research and new methods to bridge times scales being developed in this program will contribute to the improved understanding of the bonding, protonation, electron transfer and reaction mechanisms in this region. Plane wave DFT methods have provided a means to simulate the both the electronic structure and dynamics from molecules and simple crystals to large nanoscale systems, and with the advent of exascale computing larger systems can readily be calculated along with new higher accuracy methods and novel methods to improve time-scales. However, these methods, because of their computational expense, have been limited to smaller systems sizes and short time-scales compared to classical molecular dynamics. Thus the performance of software is always an important consideration and the changing computing technologies based exascale are requiring major reformulations of our ab initio molecular dynamics and band structure codes.

This poster will focus on our recent applications and developments in three areas: 1) The development of periodic electron transfer methods for iron-(oxy-hydr)oxides. As part of this work we developed screened potentials that are defined solely from periodic boundary conditions rather than from material properties. This approach overcomes the limitations of physicists' highly-engineered approaches and makes chemistry many-body calculations (RPA, CCSD, etc.) tractable in periodic boundary conditions. 2) Improved implementations of plane-wave electronic structure methods into NWChem on hybrid HPC architectures, including exact exchange, fast localization based on real space density matrix, and the development of parallel in time algorithms. Our new exascale algorithms, which were highlighted by NERSC and [www.rdmag.com](http://www.rdmag.com), observe 1.8x speed-up of Intel Xeon Phi processor over a Haswell generation Intel Xeon processor. 3) Proposed new work on machine learning strategies for improving spectroscopic analysis using atomistic simulations. Even though advanced HPC algorithm development has made the first principles analysis of advanced light sources possible for the first time, the computation cost of AIMD is prohibitive for many projects in geochemistry. Using machine learning to regress AIMD into effective molecular dynamics potentials has the potential to greatly improve the efficiency of AIMD/spectroscopic analysis, as well as enable (non-ridiculous) quantum dynamics approaches for isotope fractionation that are able to overcome the limits of inherent structure approaches.

## Calcium, Carbon, and Oxygen Isotopic Fractionation Accompanying Carbonate Precipitation from High pH Waters at The Cedars, CA

John N. Christensen<sup>1</sup>, Donald J. DePaolo<sup>1,2</sup>, Mark S. Conrad<sup>1</sup>, James M. Watkins<sup>3</sup>, Marco Voltolini<sup>1</sup>, Shaun T. Brown<sup>1</sup> and Wenbo Yang<sup>4</sup>

<sup>1</sup>Earth and Environmental Science Area, Energy Geosciences Division, Lawrence Berkeley National Laboratory, Berkeley, CA 94720.

<sup>2</sup>Department of Earth and Planetary Science, University of California, Berkeley, CA 94720.

<sup>3</sup>Department of Earth Sciences, University of Oregon, Eugene, OR 97403

<sup>4</sup>Department of Integrative Biology, University of California, Berkeley, CA 94720.

The phenomenon of isotopic fractionation by crystal growth has been investigated through theoretical models and by laboratory experiments. Though natural Ca-carbonates have been measured for Ca isotopic composition, few studies use constrained geological situations to place measurements in a kinetic context. Here we use the ultrabasic springs at The Cedars in Northern California as a natural laboratory to study isotopic fractionation by mineral precipitation. The high pH waters, initially with ~59ppm Ca and essentially zero dissolved carbonate, precipitates Ca-carbonate of various forms through interaction with atmospheric CO<sub>2</sub>. In conjunction with Ca isotopic fractionation, we examine carbon and oxygen isotope fractionation as well. Previous investigators have noted a near 1:1 linear relationship between  $\delta^{13}\text{C}$  and  $\delta^{18}\text{O}$  for carbonates precipitated from ultrabasic waters (O'Neil and Barnes 1971, Meister et al. 2011, Leleu et al. 2016).

Over a series of field campaigns at The Cedars, fluid samples of high pH spring, spring-fed pools, and Austin Creek were collected for Ca isotopic and elemental analysis. Ca-carbonate of various textural occurrences (Ca-carbonate "floes" on pool surfaces, Ca-carbonate "snow" from pool bottoms, recent encrustations and old travertine deposits) were measured for Ca, C, and O isotopic analysis as well as characterization by XRD and SEM. The most common Ca carbonate polymorphs encountered are aragonite and calcite. We focused in particular on Ca-carbonate "floes" that form thin (< 25 microns), continuous layers at the surfaces of pools fed by high-pH springs. From SEM observations, the floes build initially from horizontally- and downward radiating sprays of aragonite crystals, which in turn are overgrown by rhombs of calcite. Since the ultrabasic spring waters as well as the pools have very low Mg/Ca molar ratios (< 0.01), the favoring of aragonite is driven by the high (>11) pH of the waters (Tai and Chen, 1998) rather than high Mg/Ca as suggested by Meister et al. (2011).

Five matched pairs of Ca-carbonate "floe" and associated pool water indicate a Ca isotopic fractionation ( $\delta^{44/40}\text{Ca}$ ) of  $-0.75 \pm 0.07$  ‰ which is indistinguishable from the fractionation ( $-0.76 \pm 0.12$ ) derived from the Ca isotopic compositions of the fluids with pH > 11 suggesting that all Ca-carbonate precipitation, independent of texture, occurring at The Cedars has a common Ca isotopic fractionation. A field-measured growth rate of the "floe" Ca-carbonate of  $6\text{-}10 \times 10^{-7}$  mol/m<sup>2</sup>sec suggests a consistency with models of 2D surface nucleation for growth and constrains the saturation state at which precipitation happens. The O and C isotopic compositions of the Ca-carbonates of all textures fall along a 1:1 line, far from the expected equilibrium compositions, a phenomenon that tests our ability to understand and model the surface kinetic and transport effects involved.

## Molecular Modeling of Nanoparticle-Water Interactions: Adsorption and Aggregation

Louise J. Criscenti<sup>1</sup>, Tuan Ho<sup>1</sup>, Andrew S. Lee<sup>1</sup>, Jeffery A. Greathouse<sup>1</sup>, Kevin Leung<sup>2</sup>, and Yifeng Wang<sup>3</sup>

<sup>1</sup>Geochemistry, <sup>2</sup>Nanostructure Physics, and <sup>3</sup>Nuclear Waste Disposal Research and Analysis Departments, Sandia National Laboratories, Albuquerque, NM 87185.

The adsorption of aqueous ions at mineral-water interfaces plays a key role in ion migration in both surface and subsurface environments. Ion adsorption experiments are frequently designed to investigate adsorption on mineral particles. In porous media such as sediments and rocks, ion adsorption is affected by variable pore sizes, pore connectivity, lower water-mineral ratios, and interfaces between different mineral particles. In contrast, ion adsorption examined by molecular simulations is usually performed on one mineral surface at a time using a slit-pore geometry.

In our research, we have used classical molecular dynamics simulation to study the adsorption of  $\text{Na}^+$ ,  $\text{Ca}^{2+}$ ,  $\text{Ba}^{2+}$ , and  $\text{Cl}^-$  ions on gibbsite edges (1 0 0), basal surfaces (0 0 1), and gibbsite nanoparticles (NP). Our results indicate that  $\text{Na}^+$  and  $\text{Cl}^-$  ions adsorb on both (1 0 0) and (0 0 1) surfaces as inner-sphere complexes, with no water molecules between the ion and the surface. In addition,  $\text{Cl}^-$  ions adsorb as outer-sphere complexes, with one water molecule between the  $\text{Cl}^-$  ion and the surface. On the (1 0 0) edge,  $\text{Ca}^{2+}$  ions adsorb as inner-sphere and outer-sphere complexes, whereas on the (0 0 1) surface, outer-sphere  $\text{Ca}^{2+}$  ions are the dominant species.  $\text{Ba}^{2+}$  ions were found as inner-sphere and outer-sphere complexes on both surfaces. Surface coverages for the cations on the gibbsite NP are always higher than those calculated for the (1 0 0) and (0 0 1) surfaces. This enhanced ion adsorption is due to the significant number of inner-sphere cations found at NP corners. These results emphasize the importance of investigating adsorption to nanoparticle corners and other types of defect sites.

Success in simulating gibbsite nanoparticles allows us to build a complex aggregate model with interparticle pores, and interparticle boundaries at the atomistic scale for future investigation of ion migration through porous media. We have developed a molecular dynamics simulation method to construct complex and realistic clay-like nanoparticle aggregates with interparticle pores and grain boundaries. Different aggregates were formed by varying the rates of dewatering or water concentrations to evaluate the effects on micro-porosity. The results suggest that slow dewatering will create more compact aggregates than fast dewatering. Furthermore, the amount of water present in the aggregates strongly affects the particle-particle interactions and hence the aggregate structure. Detailed analyses of particle-particle and water-particle interactions provided a molecular-scale view of the development of different aggregate porosities and textures. This research will be extended to investigate ion adsorption and transport through different types of complex nanoporous media.

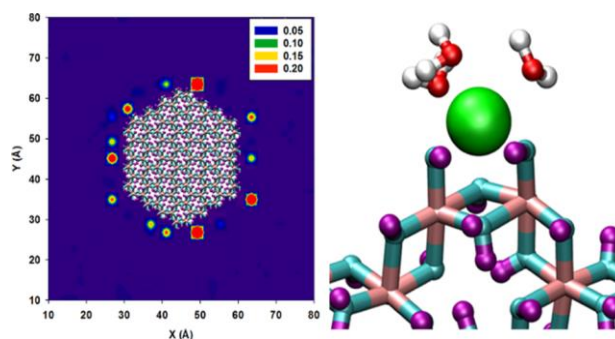


**Figure 1.** Planar density distribution of  $\text{Na}^+$  ions near the NP in a 1 M NaCl solution and snapshot showing the adsorption of a  $\text{Na}^+$  ion at a NP corner along with first-shell water molecules.

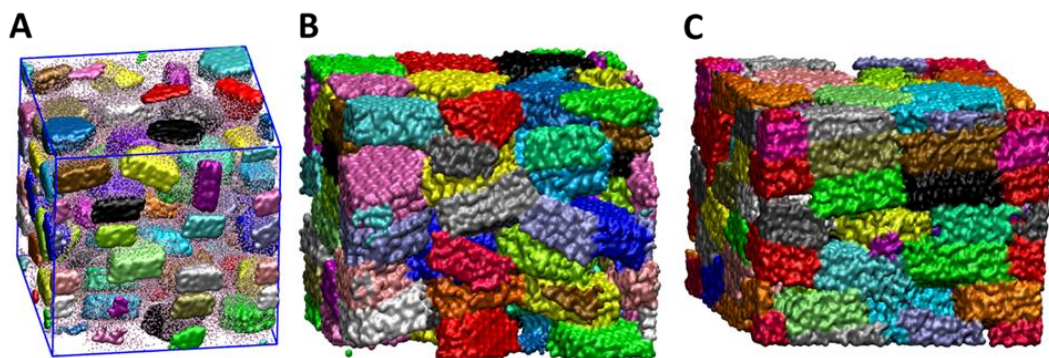


**Figure 2.** Simulation snapshot representing the starting system (A). Simulation snapshots showing the effect of 'fast' (B) and 'slow' (C) dewatering rate on aggregate structures.

- (1) Ho, T.A., Greathouse, J.A., Wang, Y. and Criscenti, L.J. (2017) Atomistic structure of mineral nano-aggregates from simulated compaction and dewatering. *Scientific Reports* 7, #15286.
- (2) Ho, T.A., Greathouse, J.A., Lee, A.S. and Criscenti, L.J. (2018) Enhanced Ion Adsorption on Mineral Nanoparticles. *Langmuir* 34, 5926-5934.

Sandia National Laboratories is a multi-mission laboratory managed and operated by National Technology and Engineering Solutions of Sandia, LLC., a wholly owned subsidiary of Honeywell International, Inc., for the U.S. Department of Energy's National Nuclear Security Administration under contract DE-NA0003525. SAND2018-7551A.

## Seawater chemistry and carbonate mineral growth

Donald J. DePaolo<sup>1,2</sup>, Laura N. Lammers<sup>1,3</sup>

<sup>1</sup>Energy Geosciences Division, Lawrence Berkeley National Laboratory, Berkeley, CA 94720. <sup>2</sup>Department of Earth and Planetary Science, University of California, Berkeley, CA 94720. <sup>3</sup>Dept. of Environmental Science, Policy and Management, University of California, Berkeley, CA 94720.

The nucleation and growth of calcite and related CaCO<sub>3</sub> polymorphs from aqueous solutions has been a subject of investigation for decades because of its importance to marine life and the geochemical cycles that regulate Earth's climate. Carbonate minerals are viewed as recorders of past Earth surface conditions, such as the chemical composition and temperature of the oceans. Continuing study is necessitated by the unusual complexity of the carbonate system, the fact that biogenic carbonate is not formed near equilibrium, and that seawater-like fluids contain dissolved species that can inhibit or otherwise modify mineral growth. Organisms that grow carbonate shells practice controlled synthesis where fluid composition is adjusted to regulate growth conditions.

The isotopic composition of the Ca, C, and O, plus the concentrations and isotopic compositions of cation impurities Mg, Sr, Mn, U, Cd, and anion impurities SO<sub>4</sub> and BO<sub>3</sub> are all used to provide information about past mineral growth conditions or seawater composition. All are subject to kinetic fractionation effects, and many interact with one another during growth.

Research over the past two decades has established that seawater composition has shifted on ca. 100 million year timescales<sup>1</sup>. The modern ocean has Mg/Ca = 5.3, SO<sub>4</sub>/Ca = 2.7, pH ≈ 8.1, and Ca/CO<sub>3</sub><sup>2-</sup> ≈ 50. In the mid-Cretaceous and in much of the Paleozoic these values were typically 1, 0.3, 7.6, and 500. All of these variables affect calcite growth and partitioning of impurity elements and isotopes during growth. For example, in the Cretaceous ca. 100 million years ago, calcite growth would have been less inhibited by Mg and SO<sub>4</sub>, which coupled with lower pH and higher temperature, means that calcite would precipitate at the same rate at lower supersaturation (closer to equilibrium). This effect could be partly offset by the higher Ca/CO<sub>3</sub><sup>2-</sup>. Changing seawater composition also affects fractionation of <sup>44</sup>Ca/<sup>40</sup>Ca, <sup>18</sup>O/<sup>16</sup>O, Sr/Ca, and Mg/Ca during calcite growth<sup>2,3</sup>.

Available data suggest that seawater Sr/Ca has not changed much over the past 250 m.y., although this inference requires knowledge of the dependence of K<sub>Sr</sub> on temperature and Ca/CO<sub>3</sub><sup>4,5</sup>. However, bulk carbonate Sr/Ca in 100 Ma Cretaceous marine carbonate sediments is about 1/3 the value in analogous more recent sediments, which can be considered *prima facie* evidence that carbonate formation conditions were different then. This Sr/Ca variation would be consistent with carbonate shell/test formation being at closer-to-equilibrium conditions in Cretaceous time. There are then also implications for O isotope fractionation; the simplest conclusion being that Cretaceous seawater temperatures were higher than currently estimated. The effect of lower Cretaceous seawater Mg/Ca would also move inferred paleotemperatures to higher values. Fully accounting for all the effects of seawater composition (including aqueous Ca/CO<sub>3</sub>) remains challenging, but paleoseawater and temperature reconstruction presents an interesting test of our understanding of the controls on carbonate mineral growth.

References: (1) Lowenstein et al. (2014) *Treatise on Geochemistry* (2) Watkins et al (2017) *RiMG* (3) Lammers and Mitnick (2018) *GCA* (in review) (4) Turchyn and DePaolo (2018) *AREPS* (in review) (5) Zhang and DePaolo (2018) (in prep)

## Complexity in Metal-Mineral Interactions

Ke Yuan<sup>1</sup>, Erika Callagon La Plante<sup>1</sup>, Kathryn L. Nagy<sup>3</sup>, Neil C. Sturchio<sup>3</sup>, Sang Soo Lee<sup>1</sup>, Paul Fenter<sup>1</sup>

<sup>1</sup>Chemical Sciences and Engineering, Argonne National Laboratory, Argonne, IL 60439<sup>2</sup> Dept. of Earth and Environmental Sciences, University of Illinois Chicago, Chicago IL, 60607<sup>3</sup> Department of Geological Sciences, University of Delaware, Newark, DE 19716

The interaction of heavy metals with mineral surfaces controls its transport in the near surface environment through reactions including metal adsorption, incorporation, heterogeneous growth of secondary phases, and morphological changes in the mineral phase. Here, we review recent work in two areas: otavite films on carbonates where we demonstrate that epitaxy of thin mineral films influences their kinetic stability dissolution reactions; and the interaction of Pb with calcite surfaces where the solution transport of the reactants leads to dramatic changes in the reactivity through the precipitation of cerussite and the evolution of the calcite surface topography.

The interaction of Cd with calcite and dolomite surfaces has been studied to understand the relationships between the epitaxial otavite film with the carbonate substrate. The focus of this work is understanding how lattice strain in the epitaxial otavite films influences its growth and stability. Otavite films initially grow as coherently strained films up to a “critical thickness” of ~5 monolayers (ML, or 17 Å thickness), followed by the development of dislocations leading to a strain-relieved film<sup>1-2</sup>. We find that the sequestration of Cd of the thin otavite films depends sensitivity on the film thickness<sup>3</sup>. Coherently strained <2 ML-thick films have a net dissolution rate that is ~2-fold smaller than that of coherently strained films with thickness of up to 4 ML, thicker (>4 ML) strain-relieved films, or bulk otavite. This indicates that the epitaxy of the strained otavite film contributes to its kinetic stability.

The interaction of Pb with calcite surfaces leads to dramatically different behavior. At the highest Pb concentrations, we observe a mineral replacement reaction in which cerussite forms as a result of a coordinate dissolution-precipitation process<sup>4</sup>. These cerussite films exhibit morphological texture but not epitaxial alignment. At lower Pb concentrations, we observe that cerussite nucleates within partially confined areas which we associate with limited solution transport and local supersaturation<sup>5</sup>. We also find that the faces of the dissolving calcite rhombs develop large-scale pyramidal dissolution structures that consist of calcite<sup>5</sup>. We speculate that these structures develop through the pinning of the surface steps by adsorbed Pb. These results are in stark contract to what is found in the absence of Pb, where calcite rhombs preferentially dissolve near corners/edges, leading to rounded shapes with continued dissolution.

### References:

- (1) Callagon, E. B. R.; Lee, S. S.; Eng, P. J.; Laanait, N.; Sturchio, N. C.; Nagy, K. L.; Fenter, P., Heteroepitaxial growth of cadmium carbonate at dolomite and calcite surfaces: Mechanisms and rates. *Geochim Cosmochim Acta* **2017**, 205, 360-380.
- (2) Callagon-La Plante, E.; Eng, P. J.; Lee, S. S.; Sturchio, N. C.; Nagy, K. L.; Fenter, P., Evolution of Strain in Heteroepitaxial Cadmium Carbonate Overgrowths on Dolomite **2018**, *Crystal Growth & Design* 18(5), 2871-2882.
- (3) Callagon-La Plante, E.; Lee, S. S.; Eng, P. J.; Stubbs, J. E.; Fenter, P.; Sturchio, N. C.; Nagy, K. L., Dissolution kinetics of epitaxial cadmium carbonate overgrowths on dolomite, **2018**, *Environmental Science and Technology*, in review.

(4) Yuan, K.; Lee, S. S.; De Andrade, V.; Sturchio, N. C.; Fenter, P., Replacement of Calcite ( $\text{CaCO}_3$ ) by Cerussite ( $\text{PbCO}_3$ ). *Environ Sci & Technol* **2016**, 50 (23), 12984-12991.

(5) Yuan, K.; Lee, S. S.; Wang, J.; Sturchio, N. C.; Fenter, P., Templating Growth of a Pseudomorphic Lepidocrocite Microshell at the Calcite-Water Interface. *Chemistry of Materials* **2018**, 30 (3), 700-707.

## The Dynamics of Confined Aqueous Solutions

Baptiste Dazas<sup>1,2\*</sup>, Chris Colla<sup>3\*</sup>, Marzena Prus<sup>4</sup>, Karolina Kedra-Krolik<sup>4</sup>, Piotr Zarzycki<sup>3</sup>, Apple Li<sup>5</sup>, Ricardo H. R. Castro<sup>5</sup>, Ian C. Bourg<sup>1</sup> and Benjamin Gilbert<sup>3</sup>

<sup>1</sup> Department of Civil and Environmental Engineering, Princeton University<sup>2</sup> Université de Poitiers, CNRS, UMR 7285 IC2MP, Equipe Hydrasa, Poitiers, France <sup>3</sup> Energy Geoscience Division, Lawrence Berkeley National Laboratory, Berkeley CA<sup>4</sup> Polish Academy of Science, Warsaw, Poland <sup>5</sup> Peter A. Rock Thermochemistry Laboratory and NEAT ORU, University of California – Davis, Davis CA. \* equal co-authors

In the natural world, confined aqueous solutions are found in surface wetting films, in the interlayer spaces of swelling clay minerals and within nanoporous rocks including shales and diatomite. Confinement in polar or non-polar environments alters the hydrogen bonding network of liquid water, leading to changes in thermodynamic properties (*e.g.*, water chemical potential and phase transition temperatures) as well as long-timescale dynamics (*e.g.*, diffusivity and viscosity). Confinement likely also has significant effects on the properties of solutes, as the alteration of the static dielectric constant alters ion hydration enthalpies. Presently, however, the chemical effects of confinement are poorly understood. We are using a range of experimental and molecular simulation methods to couple thermodynamic descriptions of these aqueous fluids to the dynamics and geochemical properties of solutes within them.

Dielectric relaxation spectroscopy (DRS) is a versatile approach for studying the structure and dynamics of aqueous solutions. DRS measures the frequency-dependent polarizability and conductivity of any medium in response to an oscillating electric field. Bulk liquid water exhibits a characteristic Debye relaxation that is a collective response of the electronic dipoles of water molecules interacting through a hydrogen bonding network. DRS of aqueous solutions is sensitive to any process, solute or substrate that influences the hydrogen bond network. We illustrate the strong effects of confinement on water relaxation in smectites and diatomite. Using DRS and molecular dynamics (MD) simulations we identify two distinct water species within synthetic smectites each with characteristic relaxation timescales that are significantly reduced relative to bulk water. Surprisingly, water in diatomite exhibits faster relaxation timescale, which we tentatively interpret as evidence of hydrophobic porosity. The next step is to relate interfacial water properties with the nature and strength of interactions with mineral surfaces and any sorbed cations. We report preliminary data from combined water adsorption isotherms and water adsorption calorimetry that can provide a complete thermodynamic characterization of interfacial water.

## Spherulites, sprinkles, and concentric rings in coral skeletons

Chang-Yu Sun<sup>1</sup>, Cayla A. Stifler<sup>1</sup>, Jun A. Y. Zhang<sup>1</sup>, Tal Zaquin<sup>2</sup>, Tali Mass<sup>2</sup>, Stefano Goffredo<sup>3</sup>, Giuseppe Falini<sup>4</sup>, Matthew A. Marcus<sup>5</sup>, Pupa U. P. A. Gilbert<sup>1,6</sup>

1. Department of Physics, University of Wisconsin, Madison, WI 53706, USA
2. Marine Biology Department, University of Haifa, Mt. Carmel, Haifa 31905, Israel
3. Marine Science Group, Department of Biological, Geological and Environmental Sciences, Alma Mater Studiorum – University of Bologna, 40126 Bologna, Italy
4. Department of Chemistry, Alma Mater Studiorum – University of Bologna, 40126 Bologna, Italy
5. Advanced Light Source, Lawrence Berkeley National Laboratory, Berkeley, CA 94720, USA
6. Departments of Chemistry, Geoscience, Materials Science, University of Wisconsin, Madison, WI 53706, USA

**Abstract:** Coral skeletons have long been assumed, based on their morphology, to grow spherulitically. Spherulites are polycrystalline structures with acicular crystals radiating from common centers and exhibit non-crystallographic branching (NCB), that is, narrow distributions of misorientation angles of the crystal *c*-axis across grain boundaries. We examined coral skeletons of 10 diverse species with nano-scale crystal orientation analyses using Polarization-dependent Imaging Contrast (PIC) mapping with 60-nm pixel resolution, to explore whether diverse coral species always grow aragonite (CaCO<sub>3</sub>) spherulites in their skeletons. Indeed all of them show spherulites, but, surprisingly, we discovered that entirely different structures also exist in some of the species, including 0.2 – 2 μm, randomly oriented, equant crystals termed sprinkles, and 5 – 20 μm-thick concentric rings. All three structures are shown in Figure 1. Quantitative misorientation measurements confirmed that sprinkles differ from spherulites. Inspired by the observation of sprinkles, we propose a new mechanism for spherulite formation, termed biased Ostwald ripening, in which smaller sprinkles are consumed by larger spherulitic crystals, and this selection is biased in favor of radially oriented *c*-axes. These results provide a new understanding of coral biomineralization and spherulitic growth in general, which is important for further investigations of other spherulitic biominerals such as eggshells, otoliths, and kidney stones, for geologic mineral spherulite growth in geology, and synthetic crystal growth in materials science.

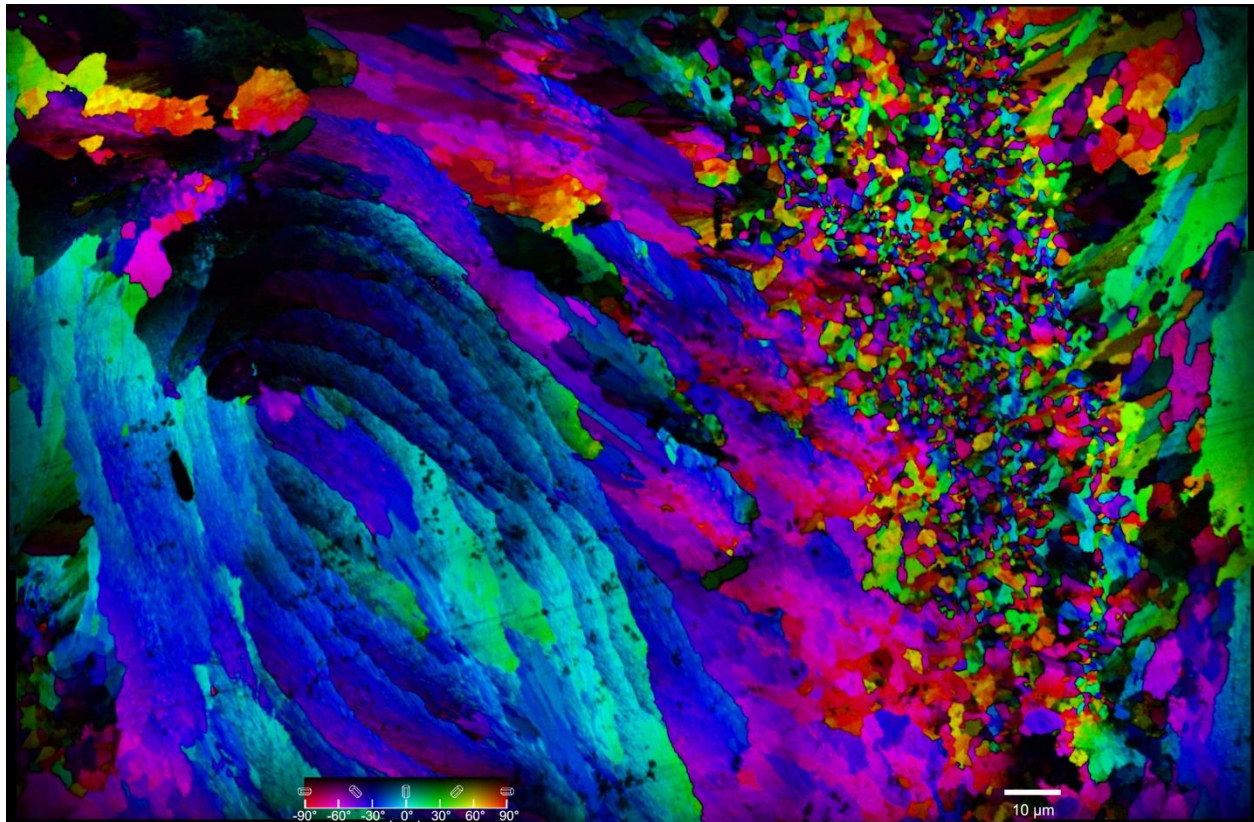


Figure 1. Polarization-dependent Imaging Contrast (PIC) map of the polished surface of an *Acropora* coral skeleton. In this PIC map color quantitative displays crystal orientations as shown in the color legend, and thus reveals previously known and new structures: (1) spherulites at the center of the image, where color changes gradually from pixel to pixel, e.g. from red to magenta to blue; (2) Newly discovered “sprinkles” on the right, randomly oriented and colored; (3) Concentric rings on the left, where orientations and colors change gradually again, from blue to cyan to green, but these “spherulites” are not at all spherical nor conical, they are concentric cylindrical layers.

## Modeling of Adsorption and Vibrational Properties at Hydroxylated Mineral Surfaces

Jeffery A. Greathouse<sup>1</sup>, Jacob A. Harvey<sup>1</sup>, Tuan A. Ho<sup>1</sup>, Kevin Leung<sup>2</sup>, Andrew S. Lee<sup>1</sup>, Louise J. Criscenti<sup>1</sup>, Rafael I. Gonzalez<sup>3</sup>, and Cliff T. Johnston<sup>4</sup> <sup>1</sup>Geochemistry and <sup>2</sup>Nanostructure Physics Departments, Sandia National Laboratories, Albuquerque, NM 87185; <sup>3</sup>Universidad Mayor, Santiago 8580745, Chile; <sup>4</sup>Crop, Soil and Environmental Sciences, Purdue University, West Lafayette, IN 47907

Force field (FF) modeling of molecular-scale interactions at mineral interfaces – particularly hydroxylated surfaces and clay mineral edges – has been significantly enhanced by the extension of the ClayFF parameter set to include hydroxylated edge sites. ClayFF allows for full flexibility of the mineral phase so that local changes in surface structure upon the interaction of liquid phases and adsorbates can be accurately modeled. We have recently developed ClayFF-compatible angle bending terms for surface or edge hydroxyl groups (e.g., Al-O-H, Mg-O-H, Si-O-H), enabling simulations of pH-dependent edge sites and surfaces.<sup>1-2</sup> Here we present results for several applications using this new modeling capability: (1) vibrational properties of edge hydroxyl groups in the neutral clay mineral pyrophyllite; and (2) molecular dynamics (MD) simulation of water and ion adsorption at silica surfaces in planar, amorphous, and nanotube environments.

First, the new angle bending parameters for surface hydroxyl groups are evaluated by comparing infrared vibrational spectra of pyrophyllite edge surfaces predicted by ClayFF with quantum (density functional theory, DFT) calculations and experiment. Vibrational modes of edge hydroxyl groups are difficult or impossible to isolate from those in the interior or even adsorbed water. However, deuteration of these groups by exposure to D<sub>2</sub>O vapor and subsequent dissociative D<sub>2</sub>O adsorption could enable the measurement of vibrational modes of OD groups due to a mass shift from deuterium atoms. Using both DFT and FF methods, we have modeled the infrared spectra of edge OH groups in pyrophyllite and the shift in these frequencies upon deuteration.

Modeling the adsorption of aqueous cations in silica slit pores aids in the interpretation of associated batch adsorption experiments using mesoporous silica and alumina, in which cation adsorption varies significantly with pore size.<sup>3</sup> We initially evaluate the degree of negative charge delocalization at deprotonated surface sites by comparing cation adsorption energies from MD simulations using ClayFF and DFT. We also present a methodology for creating more realistic model surfaces for amorphous silica, rather than the planar models typically used to simulate such surfaces. Fluid interactions at several silica surfaces are then simulated, including amorphous silica with low and high surface hydroxyl concentration, and the interior surface of imogolite nanotubes.

(1) T. R. Zeitler, J. A. Greathouse, J. D. Gale and R. T. Cygan. (2014) Vibrational Analysis of Brucite Surfaces and the Development of an Improved Force Field for Molecular Simulation of Interfaces. *J. Phys. Chem. C*, 118, 7946.

(2) M. Pouvreau, J. A. Greathouse, R. T. Cygan and A. G. Kalinichev. (2017) Structure of Hydrated Gibbsite and Brucite Edge Surfaces: DFT Results and Further Development of the ClayFF Classical Force Field with Metal–O–H Angle Bending Terms. *J. Phys. Chem. C*, 121, 14757.

(3) Knight A.W., Tigges A.B., Ilgen A.G. (2018) Adsorption of Copper on Mesoporous Silica: The Effect of Nano-scale Confinement. *Geochem. Trans.*, 19, 13.

## Formation Mechanisms, Crystal Structure, and Interfacial Reactivity of (Mixed) Metal Sulfide Nanoparticles Produced via Biological versus Abiotic Systems

Jie Xu, Muammar Mansor, Mitsu Murayama, and [Michael Hochella](#) (Virginia Tech)

Previous reports to the DOE have highlighted our discovery of differences in formation mechanisms of ZnS nanoparticles through biotic and abiotic pathways and in the presence and absence of Cu. In the past year, our focus has shifted to the characterization of mixed Fe-Cu sulfide nanoparticles produced via biotic (in the presence of microbial cells, specifically *Desulfovibrio vulgaris* strain DSM 644, a sulfate-reducing bacterium which is ubiquitous in nature) and abiotic (in the absence of microbial cells) pathways. The formed Cu-rich sulfide nanoparticles, covellite (CuS) in particular, showed distinct variations in crystal size, morphology and composition from solutions of different initial Fe-to-Cu ratios, in both the biological and abiotic scenarios. For the abiotic system, smaller CuS nanostructures (sized below 50 nm) composed of nanoparticles, nanorods and nanoplatelets were formed in the absence of Fe(II). In the presence of small amounts of Fe(II) (i.e., with an initial ratio of 1Fe:5Cu), more crystalline nanoplatelets of covellite were formed and they reach up to 200 nm in size. Further addition of Fe(II) in the synthesis resulted in chalcopyrite (CuFeS<sub>2</sub>), which is considered an extremely stable phase even under oxidized conditions. The presence of *Desulfovibrio* modified the formed Cu-Fe-sulfides moderately in terms of size, morphology and phase. For example, chalcopyrite formation started at lower initial Fe content compared to the abiotic pathway. Overall, these observations indicated that the identity and reactivity of nanoparticles are impacted by the presence of multiple metal ions and *Desulfovibrio*. These findings, the very first of their kind along with our work in the ZnS system, provide a fascinating and useful reference point for the discussion on the type and reactivity of nanoparticles that are formed in nature.

Additionally, preliminary data are being collected for the mixed Fe-Ni and Fe-Co sulfide nanoparticles. In the presence of pure Co, nanocrystalline cobalt pentlandite (Co<sub>9</sub>S<sub>8</sub>) is the primary precipitate formed through both the abiotic and biotic pathways. In the presence of pure Ni, abiotic pathway produces only the thermodynamically metastable hexagonal NiS, while the biotic pathway also produces the thermodynamically stable vaesite (NiS<sub>2</sub>). Experiments are currently being performed by starting with different amounts of aqueous Fe-to-Ni or Fe-to-Co ratios, and we expect the properties of the precipitates to change considerably depending on the synthesis conditions.

We have also used the different capabilities of TEM (SAED, EDS, HR-TEM) to characterize the phase and elemental composition of these nanoparticles. For example, EDS in particular has been very helpful. We have been able to (a) characterize the Fe-to-Cu ratios in the various nanoparticles (wide range of 5-50% molar Fe over Fe+Cu even in one sample), which indicates a solid solution of Fe-Cu-S nanoparticles ranging from Fe-rich covellite to chalcopyrite, and (b) map the Fe distribution in Fe-rich covellite to gain insights as to the formation mechanism.

## Intra-Molecular Isotope Study of Light Hydrocarbons

Juske Horita Department of Geosciences Texas Tech University

Light hydrocarbons ( $C_1 - C_6$ ) are the largest fraction of petroleum hydrocarbons. Major formation mechanisms of these light hydrocarbons include microbial, thermogenic, and abiogenic origins. It has also been increasingly recognized that hydrocarbons of varying chain-lengths can be stable even under mantle conditions and that their fluxes may play a key role in the carbon dynamics of the Earth. In the past decades, gas compositions and stable isotope ratios ( $^2H/^1H$ ,  $^{13}C/^{12}C$  or  $\delta^2H$ ,  $\delta^{13}C$ ) of light hydrocarbons have been extensively utilized to investigate their origins and transport/transformation processes. Most natural compounds, including light hydrocarbons, are composed of a set of diverse isotopic molecules that differ not only in the number of isotopic substitutions, but also in the positions of isotopic substitution within a given molecule: the latter is called isotopomers, intra-molecular or position-specific isotope effects. For example, propane ( $C_3H_8$ ) contains hydrogen and carbon at two energetically non-equivalent positions, methyl ( $CH_3$ -) and methylene ( $-CH_2$ -) groups. Position-specific isotope ratios can be defined as:

$\Delta_i = \left( \frac{f_i}{F_i} - 1 \right) 1000$  (‰), where  $f$  is a fraction of heavy isotopes ( $^2H$  or  $^{13}C$ ) within a given molecule that occupies the position  $i$  and  $F$  a fraction of heavy isotopes at the position  $i$  at random distribution.

To date, we have collected nearly 50 samples of natural gases from several oil-gas fields, including both conventional and unconventional petroleum reservoirs: Permian Basin, TX, Eagle Ford Formation, TX, and Woodford shale, OK. Of those, about two dozens of samples have been determined for position-specific H and C isotope compositions of propane. Position-specific isotopic compositions of propane show very large variations, particularly for hydrogen isotopes:  $\Delta H_{2-1} = \Delta H_2 - \Delta H_1 = -204$  to  $+38$  ‰ and  $\Delta C_{2-1} = \Delta C_2 - \Delta C_1 = -4.2$  to  $+7.8$  ‰, where the subscripts 1 and 2 stand for methyl ( $CH_3$ -) and methylene ( $-CH_2$ -) groups, respectively. In the newly defined  $\Delta H_{2-1} - \Delta C_{2-1}$  cross-plot, several propane samples fall very close to a trajectory that is defined by equilibrium position-specific isotope fractionation. Calculated formation temperatures of these propane range from 80 to 240°C, which are generally consistent with the maturation levels of the host shale organic matter. Thus, position-specific isotope compositions of propane and other light hydrocarbons could serve as a single-compound isotope thermometer for the formation of natural gases.

A majority of the current data of position-specific isotope compositions of propane does not follow simple equilibrium trajectories. The measurements of bulk ( $\delta_{bulk}$ ) and position-specific isotope compositions ( $\Delta_1$  and  $\Delta_2$ ) allowed, for the first time, to calculate the isotopic compositions at specific site ( $\delta_1$  and  $\delta_2$ ) for both hydrogen and carbon isotopes of propane. A set of data from an unconventional gas reservoir from Woodford shale in Oklahoma show that a progressive increase in  $\delta^2H_2$ , but not in  $\delta^2H_1$  with the maturity levels. On the contrary, both  $\delta^{13}C_2$  and  $\delta^{13}C_1$  of the propane remain nearly constant. These contrasting behaviors of position-specific isotope compositions of propane could be due to progressive hydrogen isotopic exchange of the  $-CH_2-$  group with formation waters in the basin. Propane from some conventional reservoirs of the Permian Basin show extreme position-specific hydrogen isotope compositions:  $\Delta H_{2-1} = \delta^2H_2 - \delta^2H_1 = -187$  to  $-204$  ‰, which is opposite of equilibrium deuterium enrichments. The cause(s) of such large negative  $\Delta H_{2-1}$  values remain to be resolved.

Our first set of data for position-specific isotope compositions of light hydrocarbons discussed above clearly demonstrate that along with conventional, compositional and bulk-isotope data, position-specific isotope compositions of propane and other light hydrocarbons have the potential to provide much deeper insights into the origin and history of light hydrocarbons and sedimentary geochemistry in general

## Interfacial Geochemistry of Nanopores: Molecular Behavior in Subsurface Environments

Anastasia G. Ilgen<sup>1</sup>, Louise J. Criscenti<sup>1</sup>, Jeffery A. Greathouse<sup>1</sup>, Kevin Leung<sup>2</sup>, Andrew W. Knight<sup>1</sup>, Tuan A. Ho<sup>1</sup>, Jacob Harvey<sup>1</sup>, Austen B. Tiggles<sup>1</sup>, and Lourdes Loera<sup>1</sup> <sup>1</sup>Geochemistry Department and <sup>2</sup>Nanostructure Physics Department Sandia National Laboratories, Albuquerque, New Mexico 87185

Our goal is to develop a molecular-level understanding of interfacial chemistry inside nano-scale pores. We use experimental and model systems relevant to geological environments to address two research tasks: *Chemistry under Nano-Scale Confinement*, and *Upscaling from the Nano- to the Meso-Scale*. This presentation will highlight our recent results from nano-scale confinement studies. Specifically, we will discuss how nano-scale confinement leads to unique chemical behavior of water and other species inside nano-scale domains. We measured the thermodynamic, vibrational, and physical properties of water residing inside silica pores. In our laboratory systems we use mesoporous silica, with a narrow pore size distribution, with mean pore diameters ranging from 2 nm to 8 nm. We quantified the kinetics of adsorption and uptake of the trace metal copper ( $\text{Cu}^{2+}$ ) and the lanthanides europium ( $\text{Eu}^{3+}$ ) and lutetium ( $\text{Lu}^{3+}$ ), as well as mixtures of lanthanides. We found that when water is confined within the mesoporous silicas, its melting temperature decreases with decreasing pore size from  $-11.3\text{ }^\circ\text{C}$  in the 8 nm pore to  $-16.5\text{ }^\circ\text{C}$  in the 4 nm pore. No melting point was observed for the smallest (2.2 nm) pore, indicating that pore water remained in a liquid-like state over the temperature range of our measurements (from  $20\text{ }^\circ\text{C}$  to  $-160\text{ }^\circ\text{C}$ ). This deviation from bulk water behavior is due to restructuring of the H-bonding networks. Vibrational spectroscopy was used to quantify the variations in the molecular populations of water. We observed a systematic blue shift in the peak locations of water populations with different degrees of H-bonding under nano-scale confinement (Figure 1). These include highly H-bonded water molecules, referred to as network water (NW), intermediate water (IW), and multimer water (MW).

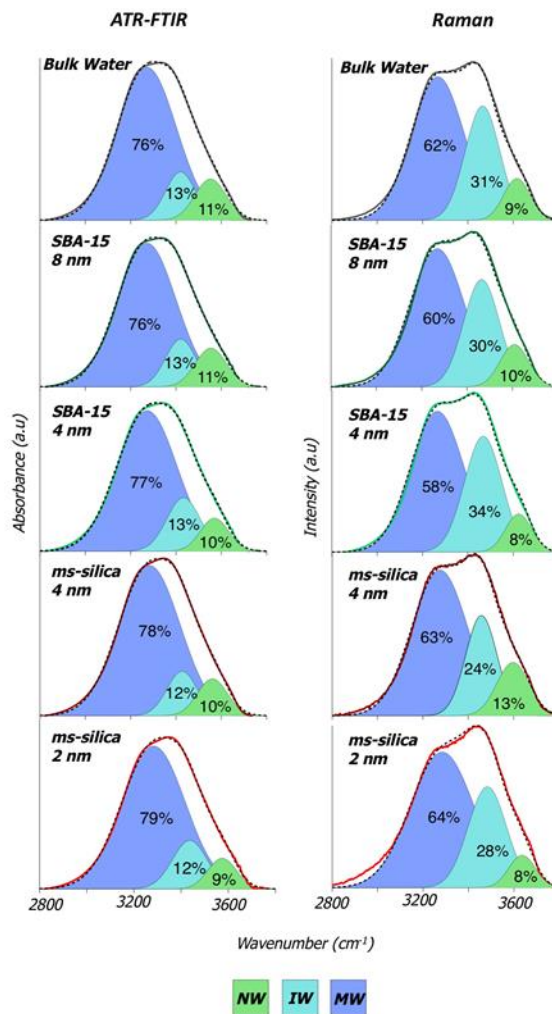
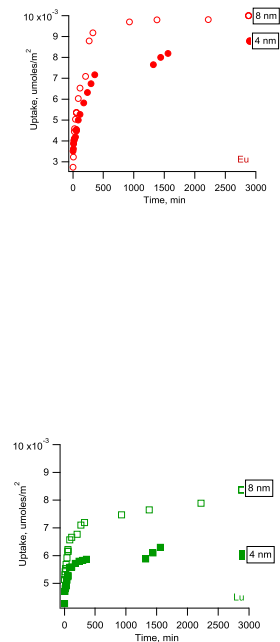


Figure 1. Systematic changes in reactivity due to nano-scale confinement in mesoporous silica: H-bonding networks in water.

These include highly H-bonded water molecules, referred to as network water (NW), intermediate water (IW), and multimer water (MW).



**Figure 2.** Systematic changes in reactivity due to nano-scale confinement in mesoporous silica: adsorption of lanthanides  $\text{Eu}^{3+}$  (top) and  $\text{Lu}^{3+}$  (bottom).

These observed deviations in the properties of water inside silica pores are also manifested in the ion adsorption behavior. With decreasing pore size, the maximum uptake of  $\text{Cu}^{2+}$  in mesoporous silica increases. The kinetics of  $\text{Cu}^{2+}$  adsorption is also faster for the 4 nm pores, compared to the 8 nm pores (Knight et al., 2018). Corresponding molecular modeling on an idealized silica surface provides additional insight into ion adsorption mechanisms. Molecular dynamics simulations at both quantum (density functional theory, DFT) and classical (ClayFF) levels of theory indicate strong adsorption of divalent  $\text{Cu}^{2+}$  and  $\text{Mg}^{2+}$  ions at a deprotonated (siloxide) surface site, while  $\text{Na}^+$  adsorption is only slightly favorable. Importantly, the quantum simulations show that a water molecule dissociates as  $\text{Cu}^{2+}$  desorbs, forming a  $\text{Cu}[(\text{OH})(\text{H}_2\text{O})_3]^+$  complex. The speciation of adsorbed copper is being investigated now using X-ray absorption fine structure spectroscopy.

We use lanthanides to further probe the kinetics of adsorption and overall uptake as a function of pore size. The ionic radii of the lanthanides decrease with increasing atomic number; and we use this systematic variation to probe the adsorption properties of nano-scale confined surfaces. The uptake of individual lanthanides on mesoporous silicas varies as a function of atomic number, or ionic radii, as well as the pore diameter (Figure 2).

## Reference

Knight A.W., Tigges A.B., Ilgen A.G. (2018) Adsorption of Copper on Mesoporous Silica: The Effect of Nano-scale Confinement. *Geochemical Transactions*, 19, 13.

## Acknowledgements

This material is based upon work supported by the U.S. Department of Energy, Office of Basic Energy Sciences, Division of Chemical Sciences, Geosciences, and Biosciences. Sandia National Laboratories is a multimission laboratory managed and operated by National Technology and Engineering Solutions of Sandia, LLC., a wholly owned subsidiary of Honeywell International, Inc., for the U.S. Department of Energy's National Nuclear Security Administration under contract DE-NA-0003525.

## **Applying Machine Learning to Probe Nonlinear Elastic Behavior in Rock and Fault-Slip Physics**

Paul Johnson Los Alamos National Laboratory

Nonlinear elastic behavior is pronounced in Earth materials from lab to Earth scale, and has important implications for earthquake hazards, for building integrity, for rock fracture networks and associated physical characteristics such as permeability. Our objectives are to better characterize nonlinear behavior of Earth materials and further, to probe the related process of fault slip applying machine learning. It is known that one of the mechanisms for nonlinear elastic behavior is slip on contact surfaces induced by acoustic or seismic vibration. These effects take place at scales ranging from dislocation ( $10^{-8}$ - $10^{-9}$  m) to meter-scale cracks and fissures, to fault scale. Other mechanisms of nonlinearity exist such as grain contact mechanics (Hertz-Mindlin) in unconsolidated material as well as in cemented granular materials such as sandstone. We are developing two promising theoretical approaches in tandem in order to better isolate the underlying physics of nonlinear elasticity to further understand and characterize its basic mechanisms. Simultaneously, we are applying machine learning to probe fault physics. A related aspect of our work just begun is applying machine learning to laboratory experimental data with the goal of extracting information about the nonlinear mechanism. This is accomplished from the continuous acoustic signals emanating from the sample during the fast nonlinear dynamics, when wave energy is still in the system, and the slow nonlinear dynamics when the wave energy has left the system and the material is recovering (this is an aging phenomenon). In summary, in this presentation I will briefly describe recent progress on theoretical aspects of nonlinear behavior of Earth materials, followed by new work applying machine learning to probing frictional behavior of fault slip and the nonlinear dynamics of Earth materials.

## **Closing the gap between experimental thermodynamic measurements and theoretical energetic data obtained from computational efforts**

Nadine Kabengi. Department of Geosciences and Department of Chemistry (Joint) Georgia State University, Atlanta, GA 30302

### Project Objectives

The overarching research goal of the initial research is to complete a systematic study of the thermodynamics properties of interfacial reactions at four MO surfaces: Rutile ( $\text{TiO}_2$ ), quartz ( $\text{SiO}_2$ ), boehmite ( $\text{AlOOH}$ ) and goethite ( $\text{FeOOH}$ ). The three specific objectives are to 1) Determine the energetics of surface protonation and deprotonation, ion exchange and ligand sorption reactions, 2) Investigate the surface charge thermodynamic properties under a range of temperature and solution chemical compositions, and 3) Develop predictive trends of the interplay between MO structure, surface coverage and surface reactivity.

### Research Highlights

Systematic work has been conducted to investigate the energetics of ions exchange and adsorption reactions on rutile, quartz, anatase, corundum, and nanohematite particles. Specifically, studies have included alkali metal ( $M^+$ :  $\text{Li}^+$ - $\text{Na}^+$ - $\text{K}^+$ - $\text{Rb}^+$ - $\text{Cs}^+$ ) and alkali earth ( $M^{2+}$ :  $\text{Mg}^{2+}$ - $\text{Ca}^{2+}$ - $\text{Sr}^{2+}$ - $\text{Ba}^{2+}$ ) cations, transition metal cations ( $\text{Al}^{3+}$ ,  $\text{Cr}^{3+}$ , and  $\text{Mn}^{2+}$ ), low molecular weight organics (citrate, oxalate, catechol) and a suite of oxyanions (sulfate, chromate, phosphate, arsenate, monomethylarsonic and dimethylarsinic acids). In all instances, the results highlighted the role hydration thermodynamics and properties play in determining, at least qualitatively, the net sign of the energetics. In addition, cation hydrolysis was found to affect the selective adsorption of cations by lowering their overall dehydration energies and favoring bond formations. Notable differences seem to appear when surfaces with contrasting chemical properties (pH of ZPNC, surface terminations, dielectric constants, etc.) are compared, e.g. rutile versus quartz and quartz versus corundum. To a large extent, rationalizing observed thermodynamics trends with surface complexation modeling (SCM) and spectroscopic techniques has been successful. Less successful, however, was the comparison of the measured enthalpies and adsorption energies with those predicted from either the temperature dependency of the SCM or density functional theory (DFT) calculations. To that effect, we have setup two model systems to examine DFT-modeled trends against experimental observations. On quartz, DFT calculations were setup to mimic  $M^+$  exchange methodologies to both  $\text{SiO}^-$  and  $\text{Si-OH}$  on quartz (101). Overall, results show that  $\text{Na}^+$ ,  $\text{K}^+$ , and  $\text{Rb}^+$  adsorption to either  $\text{Si-OH}$  or  $\text{Si-O}^-$  moieties on the quartz (101) are exothermic.  $\text{Li}^+$  adsorption is endothermic. These results agree with calorimetric results.  $\text{Na}^+$  and  $\text{K}^+$  adsorb more strongly to  $\text{Si-OH}$  on the surface than they do to  $\text{Si-O}^-$ . Conversely,  $\text{Rb}^+$  adsorbs more strongly to  $\text{Si-O}^-$  than it does to  $\text{Si-OH}$ . On ferrihydrite, DFT simulations of oxyanions adsorption have used a model nanoparticle that captures step and corner defects rather than modeling 2-D periodic surfaces. While the experimental  $\Delta H_{\text{ads}}$  and DFT  $\Delta E_{\text{ad}}$  seem to agree on the overall trend, there is a discrepancy in their overall magnitudes. Two of the main factors behind this discrepancy are the complex effect of surface coverage and the ability of the DFT modeling to realistically represent the complex experimental system.

These efforts have been limited in terms of informing and refining methodologies because of the disordered and defect nature of ferrihydrite nanoparticles where averaging of adsorption energies over surfaces, sites and mechanisms is occurring. Future work will duplicate this work on a nano-rutile surface that is compositionally simpler. A central goal from a thermodynamic point of view is to close the gap between the experimental thermodynamic measurements and theoretical energetic data.

## **Dissolution at the pore scale: comparing simulations and experiments**

Anthony Ladd, Vitaliy Starchenko, Filip Dutka, and Piotr Szymczak

University of Florida

Flow and transport in porous media are usually modeled at the Darcy scale, where the system is comprised of representative elementary volumes (REV's) described by average properties such as porosity, permeability, dispersion coefficients, and reactive surface area. Although this allows large volumes to be simulated efficiently, there are serious difficulties in developing suitable models for the properties of the REV's. When there is rapid dissolution, such as when brine pressurized with CO<sub>2</sub> encounters calcite, even the validity of the averaging process is called into doubt by the strong gradients in concentration within a single REV.

Pore-scale modeling overcomes many of the limitations of Darcy-scale models, albeit at much greater computational cost. Nevertheless, it is not yet clear that a single set of parameters – fluid viscosity, ion diffusion coefficients, and surface reaction rates – can consistently describe the dissolution samples with different pore structures. Here we describe some preliminary results of comparisons of numerical simulations with microfluidic experiments, emphasizing uncertainties in the experiments themselves, the numerical modeling of aqueous ion transport, and the characterization of surface reaction rates.

## Role of chemical-mechanical interaction in fracture size and spacing patterns

S. E. Laubach, R. H. Lander, J. E. Olson

Natural fractures are increasingly recognized to result from processes that couple mechanical failure and chemical reactions. Chemical reactions aid fracture growth through stress corrosion, whereas sealing, tip blunting, and crack-jump in response to chemical mass transfer and creep processes can impede further fracture growth and alter size and spacing patterns. Chemical-mechanical interactions affect spatial and temporal patterns of fracture network evolution and their interpretation, fault stability, and fracture and fault flow properties. Our study is testing how natural cement accumulates in fractures, how cement deposits can be used to reconstruct fracture history, and how interacting chemical-mechanical processes affect the size distribution, spatial organization, strength, porosity, and permeability of fracture arrays. Fracture mechanics has been central to interpreting opening-mode fractures in rock, but our results show that mechanics must be coupled with geochemical principles to understand how fracture porosity, spacing, size and connectivity evolve. We are developing crystal growth models that predict cement accumulation patterns and volumes in fractures and are incorporating these diagenetic features into geomechanical models of fracture pattern evolution, showing how evolving rock mechanical properties and the mechanical interaction of cement accumulation and fracture growth can influence pattern geometry and fluid flow attributes. We developed new approaches and software to quantify spatial organization. Laboratory tests we are developing provide key rock and fracture mechanical constraints. A breakthrough is our demonstration that fracture growth and diagenesis interact to create and destroy fracture porosity, and evidence of this process is preserved in quartz cement deposits in partially open fractures. We showed that using cement textures and fluid inclusion data combined with burial histories allows inference of duration and rates at which fractures open, allowing unprecedented comparison of fracture growth models with natural examples. Although our study focuses on fractures in sandstone, our results show that these structural-diagenetic principles apply to all rock types. Using fracture pattern reconstruction approaches on subsurface data sets we are testing the evolving models. But for fully testing predictions of fracture size and spatial arrangements, models require validation in special outcrops, where fractures have diagnostic features that show they are like those in the deep subsurface. This presentation focuses on outcrop and horizontal core data sets, highlighting examples where the interaction between cement deposition and fracture widening correlates with differences in many key fracture pattern attributes, including length, height, and aperture.

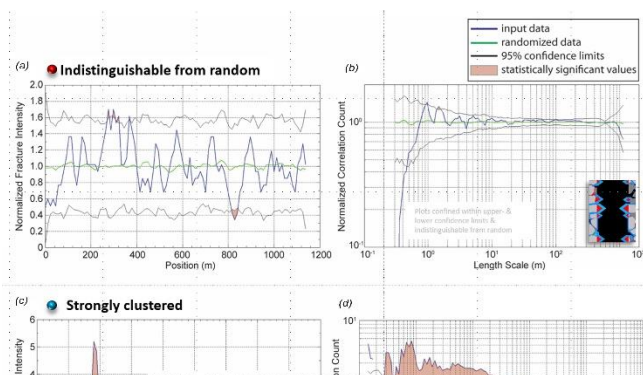


Figure 3 Increased spanning potential correlates with fracture clustering, Cretaceous Frontier Formation sandstone (after Li et al. 2018 using normalized correlation count method of Marrett et al. 2018). Spanning potential: Lander and Laubach, 2015 (insets). (a, b) Low spanning potential; clustering indistinguishable from random; (c, d) High spanning potential; hierarchical clustering.

**Selected recent references** grant DE-FG02-03ER15430 from Chemical Sciences, Geosciences and Biosciences Division, Office of Basic Energy Sciences, Office of Science, U.S. Department of Energy. For more information see project web site: <http://www.jsg.utexas.edu/sdi/>

Laubach, S.E., Lamarche, J., Gauthier, B.D.M., Dunne, W.M., and Sanderson, D.J., 2018. Spatial arrangement of faults and opening-mode fractures. *Journal of Structural Geology* 108, 2-15.

Marrett, R., Gale, J.F.W., Gomez, L., and Laubach, S.E., 2018. Correlation analysis of

fracture arrangement in space. *Journal of Structural Geology* 108, 16-33.  
doi.org/10.1016/j.jsg.2017.06.012

Li, J.Z., Laubach, S.E., Gale, J.F.W., and Marrett, R., 2018. Quantifying opening-mode fracture spatial organization in horizontal wellbore image logs, core and outcrop: application to Upper Cretaceous Frontier Formation tight gas sandstones, USA. *Journal of Structural Geology* 108, 137-156.  
doi.org/10.1016/j.jsg.2017.07.005

Hooker, J.N., Laubach, S.E., and Marrett, R., 2018. Microfracture spacing distributions and the evolution of fracture patterns in sandstones. *Journal of Structural Geology* 108, 66-79.  
doi.org/10.1016/j.jsg.2017.04.001

English, J.M., and Laubach, S.E., 2017. Opening-mode fracture systems – Insights from recent fluid inclusion microthermometry studies of crack-seal fracture cements. In Turner, J.P., Healy, D., Hillis, R.R., and Welch, M., eds., *Geomechanics and Geology: Geological Society, London, Special Publications*, 458, 257-272. doi:10.1144/SP458.1

Laubach, S.E., Fall, A., Copley, L.K., Marrett, R., Wilkins, S., 2016, Fracture porosity creation and persistence in a basement-involved Laramide fold, Upper Cretaceous Frontier Formation, Green River Basin, U.S.A. *Geological Magazine* 153 (5/6), 887-910. doi:10.1017/S0016756816000157

Ukar, E., Laubach, S.E., Marrett, R., 2016, Quartz c-axis orientation patterns in fracture cement as a measure of fracture opening rate and a validation tool for fracture pattern models: *Geosphere* 12 (2), 400–438, doi: 10.1130/GES01213.1

Fall, A., Ukar, E., Laubach, S.E., 2016. Origin and timing of Dauphiné twins in quartz cement in fractured sandstones from diagenetic environments: insight from fluid inclusions. *Tectonophysics* 687, 195-209.  
doi.org/10.1016/j.tecto.2016.08.014

Lander R.H., and Laubach, S.E., 2015, Insights into rates of fracture growth and sealing from a model for quartz cementation in fractured sandstones. *Geological Society of America Bulletin* 127 (3-4), 516-538.  
doi: 10.1130/B31092.1

## Effect of anions on the formation and uptake of Zr nanoparticles at the muscovite (001) surface

Ke Yuan,<sup>1</sup> Jacquelyn N. Bracco,<sup>1</sup> Moritz Schmidt,<sup>2</sup> L. Soderholm,<sup>1</sup> Paul Fenter,<sup>1</sup> and Sang Soo Lee<sup>1, 1</sup>  
Chemical Sciences and Engineering Division, Argonne National Laboratory, 9700 South Cass Avenue, Argonne, IL 60439; <sup>2</sup>Helmholtz-Zentrum Dresden-Rossendorf, Institute of Resource Ecology, Dresden, Germany

Predicting the stability and reactivity of multivalent cations in aqueous conditions is often challenging mainly because of their complex chemical speciation. Many multivalent cations readily undergo oligomerization, resulting in the formation of polynuclear species such as nanoparticles, whose mobilities can be controlled by the interaction with mineral surfaces. Here, we investigated adsorption of Zr nanoparticles to the basal surface of muscovite mica from acidic solutions (pH 3) containing one of four anions ( $\text{ClO}_4^-$ ,  $\text{Cl}^-$ ,  $\text{SO}_4^{2-}$ , and  $\text{HPO}_4^{2-}$ ). The results reveal the strong influence of these anions on the adsorbed coverage and distribution of Zr at the surface. The highest Zr coverage ( $4\text{--}7\text{ Zr/nm}^2$ ) was observed in  $\text{SO}_4^{2-}$  solutions, based on grazing incidence X-ray fluorescence. However, resonant anomalous X-ray reflectivity showed almost no adsorbed Zr that was structurally ordered at the surface (Fig. 1), indicating that the major mechanism for Zr uptake was simple precipitation. Adsorption behavior was clearly distinct in the  $\text{ClO}_4^-$  and  $\text{Cl}^-$  solutions where both high coverages ( $2\text{--}3\text{ Zr/nm}^2$ ) and structurally ordered Zr species were observed. In contrast, little or no Zr sorbed on the surface from the  $\text{HPO}_4^{2-}$  solution. These differences demonstrate that the interaction between nanoparticles and anions can be a critical factor in determining the fate of multivalent cations in aqueous environments.

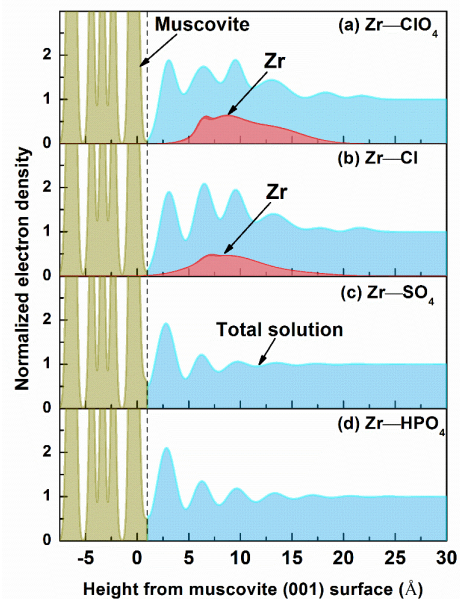


**Fig. 1:** Distribution of Zr adsorbed at the muscovite (001) – solution interface at pH 3 with monovalent

### References:

- 1) M. Schmidt, S. S. Lee, R. E. Wilson, K. E. Knope, F. Bellucci, P. J. Eng, J.E. Stubbs, L. Soderholm, and P. Fenter, *Environmental Science & Technology* **47**, 14178-14184 (2013).
- 2) S. S. Lee, M. Schmidt, T. T. Fister, K. L. Nagy, N. C. Sturchio, and P. Fenter, *Langmuir*, **32**(2), 477–486 (2016).
- 3) S. Hellebrandt, S. S. Lee, K. E. Knope, A. J. Lussier, J. E. Stubbs, P. J. Eng, L. Soderholm, P. Fenter, M. Schmidt, *Langmuir*, **32**(41), 10473–10482 (2016).

## Reactivity and Transformations of Minerals in Adsorbed H<sub>2</sub>O Films

John S. Loring, Eugene S. Ilton, Quin R. S. Miller, Edmundo Placencia-Gomez, Odeta Qafoku, Chris J. Thompson, H. Todd Schaefer, Sebastien N. Kerisit, Pascale Bénézeth, David A. Dixon, and Kevin M. Rosso

Pacific Northwest National Laboratory, Richland WA 99352

Minerals in low-water environments, such as when pore fluids are non-aqueous or at nanoparticle surfaces in the atmosphere, are covered in films of H<sub>2</sub>O that are only monolayers thick. Reactions in these films are subject to dramatically different conditions than in bulk aqueous solutions. Within films H<sub>2</sub>O is nanoconfined between the surrounding fluid or gas on one side and the mineral surface on the other. Strong hydrophilic interactions with the surface disrupt the H-bond network of bulk H<sub>2</sub>O and restrict the ability of H<sub>2</sub>O to reorient to solvate ions and facilitate diffusive mass transport for processes such as dissolution or precipitation and growth. This surface imposed structuring is progressively relaxed as the H<sub>2</sub>O film thickens, but bulk-like behavior may never be obtained because of an inadequate driving force for the formation of a liquid phase in H<sub>2</sub>O-undersaturated conditions. Despite numerous examples of H<sub>2</sub>O-limited domains in nature, we currently lack a fundamental understanding of coupled mineral dissolution, nucleation, and growth reactions in confined adsorbed H<sub>2</sub>O films. Here, we present results of three case studies that use infrared (IR), <sup>18</sup>O exchange, and impedance experiments to interrogate molecular-level controls on thin H<sub>2</sub>O film reactivity at subsurface reservoir temperatures and pressures. First, we discuss the role of H<sub>2</sub>O structure in the formation of carbonic acid in H<sub>2</sub>O films on fumed silica (SiO<sub>2</sub>) in humidified supercritical CO<sub>2</sub> (scCO<sub>2</sub>). Self-associated “liquid-like” H<sub>2</sub>O adsorbed on SiO<sub>2</sub> catalyzes the formation of carbonic acid, yet surface-structured “ice-like” H<sub>2</sub>O is unreactive within our measurement uncertainty. Second, we show the relationship between H<sub>2</sub>O structure and mobility in H<sub>2</sub>O films on forsterite (Mg<sub>2</sub>SiO<sub>4</sub>) in wet supercritical N<sub>2</sub> (scN<sub>2</sub>). Concentrations of liquid-like H<sub>2</sub>O detected by IR correlate with diffusion-related parameters measured by impedance spectroscopy. Third, we discuss the carbonation of forsterite covered in thin H<sub>2</sub>O films in humid scCO<sub>2</sub>. Although IR cannot resolve structurally distinct H<sub>2</sub>O in this system, impedance spectroscopy links diffuse-layer mobility with carbonation reactivity. This research advances a predictive understanding of complex fluid systems involving interfaces and confinement and is important for CO<sub>2</sub> utilization and storage operations, including enhanced gas recovery (EGR), geologic carbon sequestration (GCS), and enhanced geothermal systems (EGS).

## **Fusing Thermoacoustic, Electromagnetic, and Acoustic/Seismic Wave Fields for Subsurface Characterization and Imaging of Flow and Transport.**

Jose Martinez-Lorenzo, Northeastern University, Boston, MA

Accurate predictions of fluid flow, mass transport and reaction rates critically impact the efficiency and reliability of subsurface exploration and situation awareness. Quantitative dynamical sensing and imaging can play a pivotal role in the ability to make such predictions. In pursue of this, the overarching goal of this research program is to gain knowledge on the theory and experimental validation of a new unified sensing and imaging methodology for coupling electromagnetic (EM), acoustic/seismic (AC/S), and novel thermoacoustic (TA) physical fields, which handles multi-physics and multi-scale material characterization and underground imaging of fluid flow in porous media.

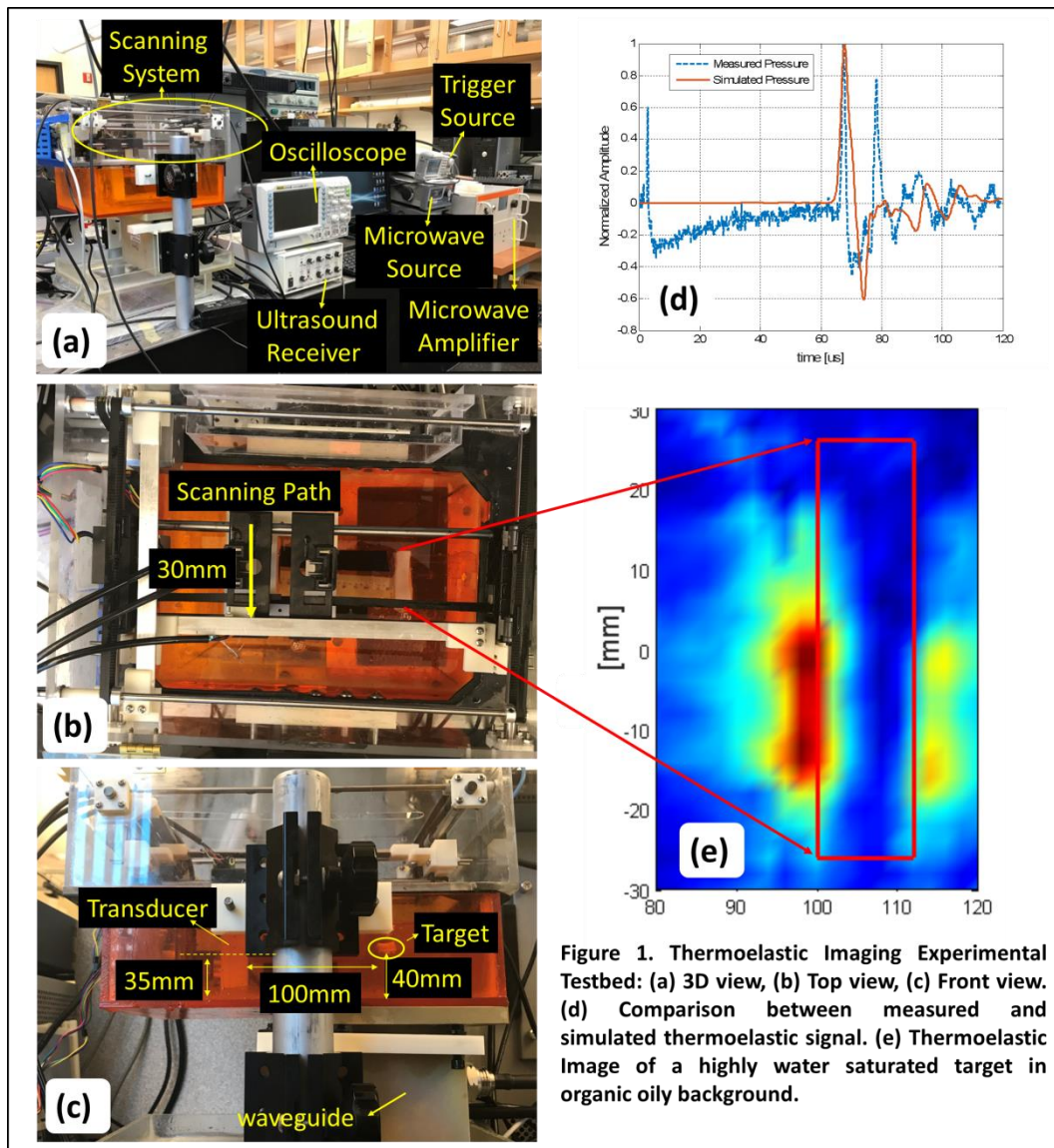
Over the last funding period, we developed a mathematical framework and carried out simulations to model thermoelastic wave generation and propagation in the time domain, so that it is possible to understand the physical limitations of thermoacoustic imaging in geophysical applications. Our multi-physics simulation is performed in three steps [1]. First, a microwave pulse is generated in the time domain. The shape of the pulse was arbitrarily designed to enable enhanced signal to noise ratio. Second, the heat transfer equation is used to account for the volumetric dilation of a target, which produces an outwardly propagating elastic wave. This equation accounts for all terms, including density, specific heat capacity, temperature, velocity of the translational motion, heat flux by conduction, heat flux by radiation, heat source, coefficient of thermal expansion, and stress tensor. However, the heat equation can be simplified for short EM pulses, so that the temperature rate only depends on the heat source, density, and heat capacity. Third, in fluid-like mediums where there is no shear wave, the solid mechanics equation that governs the wave propagation in elastic media can be approximated by the acoustic wave equation, and the heat source excites a pressure wave that propagates outwardly.

Over the last funding period, we also investigated a new 4D-coded holey-cavity structure, which leverages on information-theory principles to enhance the amount of information that is transferred between sensors and imaging domain [2]. Combining this 4D-coding of the holey-cavity with compressive sensing techniques reduces the number of receivers needed to produce images with high-spatial-resolution in both range and cross-range directions. In order to enable real-time imaging, a distributed Alternating Direction Method of Multipliers (ADMM) algorithm, capable of using norm-1 and norm-2 regularizers, has been implemented [3]. Preliminary results showed the efficacy of our approach in terms of imaging performance. Moreover, a mathematical formulation of a compressed sensing unmixing algorithm to enable enhanced petrophysical imaging was presented in [4]. In the unmixing problem, each voxel in the imaging region contains a mixture of soil, water, oil, and gas; and the goal of the algorithm is to recover this mixture proportions. This approach intrinsically accounts for the dispersion of materials and enables joint multimodal imaging without increasing the number of unknowns. This framework will be used to enable TA petrophysical characterization at the pore-scale.

An experimental testbed is also being developed in order to determine the effectiveness of our research using controlled laboratory and simulated environments. Over the last funding period, we have been able to design, build, an experimentally test a prototype capable of creating thermoelastic waves. The prototype uses an arbitrary wave generator to create a Frequency Modulated Continuous Wave pulse, which passes through a high-power microwave amplifier before it illuminates the target. This EM wave-front coding has the potential to enable our TA testbed to reach farther ranges.

- [1] Chang Liu, Ashkan Ghanbarzadeh Dagheyan, Juan Heredia Jueas, Ali Molaei, and Jose Martinez Lorenzo. "Microwave-Induced Thermoacoustic Imaging Using Compressive Sensing and a Holey Cavity," IEEE AP-S International Symposium, Boston, MA, Jul. 2018.

- [2] Ashkan Ghanbarzadeh Dagheyan, Chang Liu, Ali Molaei, Juan Heredia Juesas, and J. A. Martinez-Lorenzo. "Holey-cavity-based Compressive Sensing for Ultrasound Imaging." *Sensors*, 18(6):1674, 2018.
- [3] Juan Heredia-Juesas, Luis Tirado, and J. A. Martinez-Lorenzo. "Fast Source Reconstruction via ADMM with Elastic Net Regularization," AP-S 2018—IEEE AP-S International Symposium, Boston, MA, Jul. 2018.
- [4] Richard Obermeier and J. A. Martinez-Lorenzo. "Joint Electromagnetic and Acoustic Image Reconstruction using a Compressive Sensing Unmixing Algorithm," IEEE AP-S International Symposium, Boston, MA, Jul. 2018.



## Kinetics of D/H isotope fractionation between molecular hydrogen and water

Nicholas J. Pester <sup>a, b\*</sup>, Mark E. Conrad <sup>a</sup>, Kevin G. Knauss <sup>a</sup>, Donald J. DePaolo <sup>a, b</sup>

<sup>a</sup> Energy Geosciences Division, Lawrence Berkeley National Lab., Berkeley, CA 94720, USA <sup>b</sup> Dept. of Earth and Planetary Science, University of California, Berkeley, CA 94720, USA \*corresponding email: njpester@lbl.gov

At equilibrium, the D/H isotope fractionation factor between H<sub>2</sub> and H<sub>2</sub>O ( $\alpha_{\text{H}_2\text{O}-\text{H}_2(\text{eq})}$ ) is a sensitive indicator of temperature, with implications for geothermometry in natural springs and gas discharges. However, measured D/H values in springs may underestimate the subsurface temperatures of origin due to partial re-equilibration of H<sub>2</sub> during ascent and cooling. We present new experimental data on the kinetics of D-H exchange for H<sub>2</sub> dissolved in liquid water at temperatures below 100°C. Comparing these results with previously published data obtained under ideal gas conditions (up to 400 °C), we derive a consistent activation energy of 52 kJ/mol, and the following rate expressions;

$$\ln k = 9.186 - 6298 / T \quad k_1 = [\text{H}_2\text{O}] 9764.61 * \exp(-6298 / T)$$

where  $T$  is absolute temperature (K),  $k$  is the universal rate constant ([L/mol] / hr), and  $k_1$  is a pseudo-first-order constant (hr<sup>-1</sup>) applicable to water-dominated terrestrial systems by constraining [H<sub>2</sub>O] as the density of H<sub>2</sub>O (in mols/L) at the  $P$ - $T$  of interest. The density-dependent rate constant accounts for the disparity in kinetics attending phase changes (boiling), exemplified by  $1/k_1$  at 100 °C of ~2 days for H<sub>2</sub> dissolved in liquid H<sub>2</sub>O, versus ~7 yrs for H<sub>2</sub> in saturated steam. This difference explains the high variability of  $\delta\text{D}_{\text{H}_2}$  observed in fumarolic gases. Fluids actively convecting in the crust frequently reach  $T > 225$  °C, where  $\alpha_{\text{H}_2\text{O}-\text{H}_2(\text{eq})}$  is rapidly attained (<1 hr). We compare fractionation values measured in natural fluids ( $\alpha_{\text{OBS}}$ ) with kinetic models that simulate how  $\alpha_{\text{OBS}}$  diverges from  $\alpha_{\text{H}_2\text{O}-\text{H}_2(\text{eq})}$  as upwardly advecting fluids cool. Data from deep-sea hydrothermal systems reveal microbial catalysis of D-H exchange towards equilibrium once fluids cool below ~60 °C. Kinetic models fit to fluids from Yellowstone Park and the Lost City (deep-sea) vent field, both recovered at ~90 °C, require respective transit times of ~7 hrs and ~11 days between higher temperature reaction zones and the surface to match the observed isotopic disequilibrium. Factoring in estimates of the subsurface depth of origin, however, suggests similar mean fluid flow rates (10s of meters / hr). The H<sub>2</sub> measured in continental alkaline springs and Precambrian shield gases is generated at lower  $T$ , and  $\delta\text{D}_{\text{H}_2}$  values generally appear closer to equilibrium with H<sub>2</sub>O at the  $T$  of sampling. However, depending on residence time, kinetic isotope effects associated with ongoing H<sub>2</sub> production may not yield  $\alpha_{\text{H}_2\text{O}-\text{H}_2(\text{eq})}$ , and we calculate maximum residence times to apparent equilibrium of 1.3 yrs at 50 °C, 9 yrs at 25 °C, and 35 yrs at 10 °C. A similar calculation applied to Antarctic brines, where  $\alpha_{\text{OBS}} \ll \alpha_{\text{H}_2\text{O}-\text{H}_2(\text{eq})}$ , yields 349 yrs (-13 °C), a time shorter than the fluids have been isolated (2.8 ka), which requires considering kinetic isotope effects associated with H<sub>2</sub> destruction or loss.

## Understanding Photoexcited Charge Transport Reactivity at Geochemical Nanoparticle Interfaces

Micah P. Prange and Kevin M. Rosso

Physical Sciences Division, Pacific Northwest National Laboratory, Richland, Washington 99352, United States

Mineral nanoparticles are ubiquitous at the Earth's near-surface, and their capacity for light harvesting is profound. A key class of photoactive materials is semiconducting metal oxides, most of which naturally occur in nanophases that, because of their chemical stability, are highly persistent. As the preponderance of mineral nanoparticle influence in natural processes is becoming increasingly recognized, more attention has been focused on the associated photochemical fluxes of redox active species like Cu, Fe, and Mn in natural systems. While realization of the ubiquity and importance of natural metal oxide nanoparticles in photogeochemical roles is growing, the current understanding of the magnitude of their influence is based on limited experimental work and especially limited theoretical work. Due to the lack of comprehensive knowledge about the efficiency of natural photocatalytic processes at particle interfaces, the true extent of the role of nanoparticulate minerals has so far remained difficult to quantify. In particular, there is no predictive knowledge of the quantity of photocurrent produced in Earth-abundant nanoparticles or the resulting (bio)geological metal fluxes.

We propose research to develop a predictive understanding of nanoparticulate oxide photoreactivity that underlies the commanding role of this reaction pathway in natural Fe cycling. The proposed work aims to calibrate theory for hematite charge carrier transport, which occurs by a polaronic hopping mechanism, with an attendant suite of consistent measurements of photocurrent and photoinduced reductive dissolution flux as a function of nanoparticle morphological and compositional properties. We believe this novel strategy of following photodeposited energy step-by-step to larger time and length scales into collective carrier dynamics at the particle level will be broadly useful and impactful for understanding and predicting radiation-induced chemical kinetics, thereby serving as a model of how computational theory can be harnessed to answer scientific questions about systems that are too complicated to model directly at an atomistic level.

These goals will be achieved by constructing a first-ever quantitative multiscale model of photocarrier creation, motion, and destruction based on state-of-the-science *ab initio* calculations that will be used to inform whole-particle simulations of collective carrier dynamics that account for the effects of particle size, shape, and composition. The model will be built from computed parameters (e.g. formation energy and migration energy barriers for polarons). The model will be calibrated and refined by comparison with complementary systematic experiments including synthesis of ensembles of precision hematite nanoparticles that will facilitate the independent variation of size and morphological properties. To connect with the excitation dynamics, transient absorption spectroscopy will be performed on both synthetic nanoparticle solutions and natural hematite crystals which will be mounted in cells to allow the application of DC external fields. Finally, we will perform experiments to monitor the dependence of the rate of photoreductive hematite dissolution on nanoparticle properties using wet chemical analyses and colorimetric indicators for ferrous Fe such as ferrozine assays.

## Swarm Transport in Fractures and Porous Media

Laura J. Pyrak-Nolte<sup>1,2,3</sup>, Chven Mitchell<sup>2</sup>, Ludwig Nitsche<sup>4</sup>

<sup>1</sup>Department of Physics and Astronomy, <sup>2</sup>Department of Earth, Atmospheric and Planetary Sciences, Purdue University, <sup>3</sup>Lyles School of Civil Engineering, Purdue University, West Lafayette, Indiana, USA

<sup>4</sup>Department of Chemical Engineering, The University of Illinois at Chicago, Chicago, Illinois

Swarm physics has the potential to control the delivery of chemically-reactive granules to targeted locations in the subsurface because swarms exhibit several interesting properties. A swarm is a dilute suspension (0.4 - 2% by weight) that exhibits coherent behavior over long transport distances at speeds 10x-10,000x faster than the settling speed of an individual particle. Our research has investigated, experimentally and numerically, swarm transport in single fractures, in porous media and in fractured porous media to determine how a swarm evolves in a constrained geometry where each particle experiences an additional drag force from the presence of fracture or pore walls, and depends on the ratio of the particle radius,  $r_{particle}$ , to the distance from the wall,  $d$ . A key aspect of swarm transport is the ability of a swarm to deform in response to changes in confinement from flow/no flow boundary conditions and from variable fracture apertures or as a swarm transport from pore bodies to pore throats, or from a porous matrix across a fracture. Swarms tend to follow the path of least resistance through fractures and porous media.

The deformability of a swarm results in enhanced transport that occurs for a range of ratios of fracture aperture to swarm diameter (from 10 to 25) where a swarm travels 2.5 times faster than equivalent (size and density) immiscible sphere released between parallel plates, and swarm bifurcations are also suppressed. The enhanced transport regime occurs because the confinement of a swarm by fracture apertures alters the shape of the swarm as it falls and suppresses the probability of a hydrodynamic instability that leads to swarm bifurcation and break up. Attempts to approximate swarms as single particles between infinite parallel plates are fundamentally in error. Swarms are collections of particles interacting through hydrodynamic forces that exhibit cohesive behavior but can also deform and reform to maintain swarms in response to topological changes or flow resistance in a 2D planar fracture. Numerical simulations show that Stokes settling is not sufficient to explain the enhanced transport behavior observed in uniform aperture fractures, and may require the addition of inertial effects in future studies.

Because of their deformability, swarms are able to pass through narrow constrictions without disrupting the swarm. By combining swarm transport with chemically activated particles, we have begun initial development of a new method to illuminate and characterize fracture flow path topology. Proof-of-concept experiments were performed on a porous medium with a single fracture. An emitting chemically-reactive particle swarm was monitored as it fell under gravity through a porous-fractured media. The speed of the granule swarm transported through a porous fractured medium varied in response to changes in confinement, moving more than 10x faster across the fracture than in the upper porous matrix. A decrease in speed observed in the lower matrix is consistent with our previous swarm studies with non-reactive particle swarms. As the reactive swarm dissolved, it generated ~3100 events in 3 minutes of transport through the fracture porous medium. This is a preliminary indication of the robustness of the source under settling conditions, and of the ability to track changes in *flow path* topology from a moving internal source. The research on swarm transport in fractured and porous media lays the groundwork for a unique opportunity to both *locate* the dominant flow path from the acoustic emissions and to *quantify/estimate* the aperture/void as the emitting swarm velocity changes as it moves through a medium.

## Advancing Understanding of Iron Oxide/Water Interfacial Reactivity Far From Equilibrium

Kevin M. Rosso<sup>1</sup>, Martin E. McBriarty<sup>1</sup>, Joanne E. Stubbs<sup>2</sup>, Peter J. Eng<sup>2</sup>, Oliver Gittus<sup>3</sup>, Guido von Rudorff<sup>3</sup>, Jochem Blumberger<sup>3</sup>, Konstantin Klyukin<sup>4</sup>, Vitali Alexandrov<sup>4</sup> <sup>1</sup>Pacific Northwest National Laboratory, Richland, WA, USA; <sup>2</sup>Argonne National Laboratory, Lemont, IL, USA; <sup>3</sup>University College London, Bloomsbury, London, England, UK; <sup>4</sup>University of Nebraska, Lincoln, NE, USA

The intrinsic physical and chemical complexity at mineral/water interfaces controls processes such as sorption/desorption, diffusion, mineral nucleation and growth, dissolution, and redox-based transformations. At the nanoscale, the structure adopted at these interfaces is often substantially different than a simple truncation of the two adjacent phases. Surface atoms, water molecules, and adsorbed ions rearrange and define a unique environment with a distinct set of chemical and physical constraints through which interfacial reactions proceed. Measurements that provide atomically precise structural models of ion and solvent arrangements are essential, but most rely on static conditions near equilibrium. The reactivity of mineral/water interfaces is thus often interpreted in terms of its structure at rest, but the reality is that the structure of relevance is the one that is adopted under reaction conditions.

This presentation will overview recent advances from experiment and molecular simulations aimed at addressing this important distinction. For example, using a novel cell, the atomic structure at the hematite (012)-electrolyte interface was measured under controlled electrochemical bias using synchrotron crystal truncation rod X-ray scattering. At increasingly cathodic potentials, charge-compensating protonation of surface oxygen groups increased the coverage of bound water while adjacent water layers displace outwardly and became disordered. Returning to open circuit potential left the surface in a persistent metastable state. Thus, the flux of current and ions across the interface is regulated by multiple electrolyte layers whose structure changes in the applied potential. The study revealed the complex environment underlying the oversimplified structure models typically used to interpret charge transfer processes at these interfaces, and the importance of condition-specific characterization for properly understanding interfacial reactivity.

In a second example, using ab initio molecular dynamics simulations we explored the mechanism and kinetics of acid-promoted iron dissolution from goethite (110) and (021) surfaces in water; a complex process involving coupled hydrolysis, surface protonation, electron transfer, and metal–oxygen bond cleavage. By employing metadynamics combined with the Blue Moon ensemble approach, we were able to examine pathways and rates of both nonreductive and reductive dissolution, with the latter process entailing an experimentally observable orders of magnitude rate increase by increasing the lability of surface Fe–O bonds through reduction of Fe<sup>3+</sup> to Fe<sup>2+</sup>. The simulations reveal the interplay between concerted internal (structural) and external (from solution) protonation steps as essential for breaking Fe–O bonds, as well as for stabilizing intermediate configurations of dissolving Fe. These processes relate to the specific structure adopted by interfacial water and near-surface goethite atoms as Fe cations transition from lattice sites to aquo ions in solution. The simulations demonstrate specifically how Fe reduction yields higher dissolution rates than the proton-mediated pathway alone, making quantitative connection with experimentally measured kinetics.

The collective findings help reveal the complex interplay between structure and reactivity during interfacial reactions that is clearly masked by simplified electrical double layer models. Interfacial structure is dynamically responsive to the nonequilibrium conditions that initiate and control the progress of charge and mass transfer reactions. Condition-specific structural characterization is important for properly understanding mechanisms of interfacial reactivity at a fundamental level. This principle applies directly to understanding the mechanism of interfacial reactions broadly.

## **A potential new proxy for paleo-atmospheric pO<sub>2</sub> from soil carbonate-hosted fluid inclusions**

Morgan F. Schaller<sup>1</sup>, Elizabeth A. Pettitt<sup>1</sup>, Todd K. Knobbe<sup>1</sup>, Daniel O. Breecker<sup>2</sup>, E. Bruce Watson<sup>1</sup>

<sup>1</sup>Earth and Environmental Sciences, Rensselaer Polytechnic Institute, Troy, NY

<sup>2</sup>Jackson School of Geosciences, University of Texas at Austin, Austin, TX

We have developed a new method for determining ancient atmospheric pO<sub>2</sub> based on the composition of soil carbonate-hosted fluid inclusions, which form in equilibrium with soil pore space gas. The concentration of O<sub>2</sub> in soil gas is controlled primarily by diffusion from the atmosphere and respiration at depth. Therefore, profiles of fluid inclusion compositions can be used with a diffusion-production model to reconstruct atmospheric O<sub>2</sub>. Here we show that carbonate hosted fluid inclusions faithfully record soil gas concentrations, and that soil pO<sub>2</sub> can be derived from the total gas contents of the inclusions. Carbonate nodules collected from profiles of two modern Vertisols near Dallas and Fairfield, TX, are used as test cases. Inclusion compositions are compared to direct soil pore space gas measurements at the Fairfield site, which were collected in septum-capped vials flushed with soil gas through PVC and stainless steel gas wells. At the UT Austin lab we separate CO<sub>2</sub> from air and O<sub>2</sub> from Ar using He carrier gas in an Agilent GC and measure each gas individually using a TCD. Fluid inclusions are measured at RPI by an online crushing technique that physically ruptures inclusions into a custom-built quadrupole mass spectrometer where all the gases are measured simultaneously. We quantify pO<sub>2</sub> using a matrix-matched calibration, and define each species as a partial pressure of the total gas released. Total CO<sub>2</sub> is corrected for carbonate speciation by measuring the relative abundance of each species by Raman Spectroscopy. When corrected for aqueous solubility using Henry's Law, the soil-carbonate hosted gas concentrations agree with the soil pore space gas concentrations to within <1% for N<sub>2</sub>, O<sub>2</sub> and CO<sub>2</sub>. The diffusion-production model predicts modern atmospheric pO<sub>2</sub> of 21%, validating the method.

## Genesis, Storage, and Leakage of Shale Gas

Arndt Schimmelmann ([aschimme@indiana.edu](mailto:aschimme@indiana.edu)), Maria Mastalerz ([mmastale@indiana.edu](mailto:mmastale@indiana.edu)), and Juergen Schieber ([jschiebe@indiana.edu](mailto:jschiebe@indiana.edu)), Indiana University, Bloomington, Indiana. U.S. Department of Energy, Basic Energy Sciences, Grant No. DE-SC0006978, 8/1/11 – 7/31/19.

Shales are important source and reservoir rocks for hydrocarbons (shale gas, oil). The three research goals of this project encompass: (1) Testing of shales' ability to generate thermogenic gas (or natural gas via catalysis) at relatively low temperatures (60, 100 and 200 °C) and different pressures (ambient, 100 MPa, 300 MPa) over months to years; (2) Quantification of the character and development of porosity in organic-rich rocks as a function of organic matter content, type of organic matter, thermal maturity, and the degree of compaction; and (3) Evaluation of the outgassing of methane from shales into the atmosphere and its potential contribution to global warming by delivering potent methane greenhouse gas.

In our study of gas generation via catalysis, we have demonstrated that low temperature (60 and 100 °C) and long-term (6 months to 5 years) heating of pre-evacuated and sterilized low-maturity shales and coals containing kerogen Types I (Mahogany Shale), II (Mowry Shale and New Albany Shale), and III (Springfield Coal and Wilcox Lignite) can yield methane volumes that are 5 to 11 orders of magnitude higher than the theoretically predicted yields from kinetic models of thermogenic methane generation (Fig. 1; [Wei et al., 2018](#)). In the absence of microbial methane generation and at temperatures not high enough for a thermogenic pathway, these results strongly suggest that generation of such volumes of methane gas involves catalytic methanogenesis. Furthermore, our experimental results suggest that catalytically generated hydrocarbons may explain the occurrence of some non-biogenic natural gas accumulations where insufficient thermal maturity contradicts the conventional thermal cracking paradigm. Extrapolation of the observed rate of catalytic methanogenesis in the laboratory suggests that significant amounts of sedimentary organic carbon can be converted to relatively dry natural gas over tens of thousands of years in sedimentary basins at temperatures as low as 60 °C.

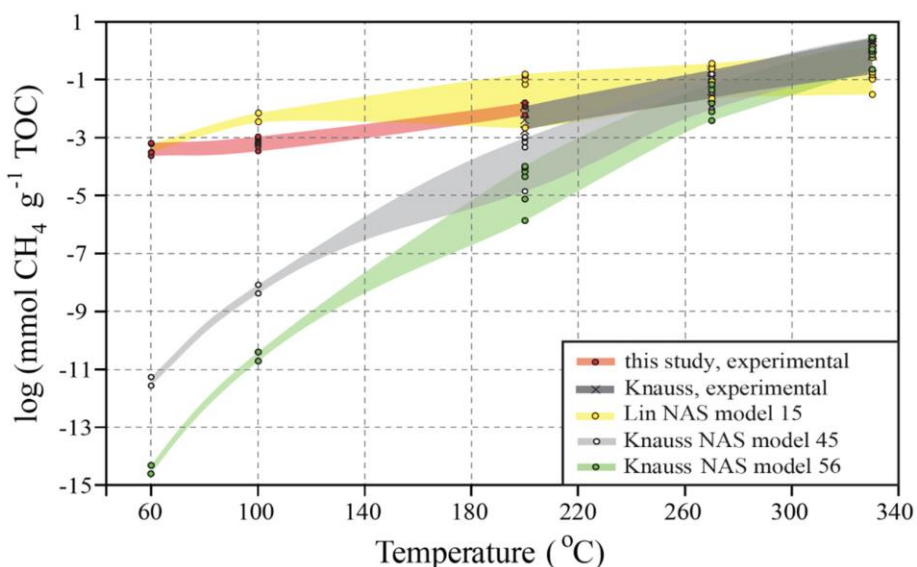


**Fig. 1.** Crossplot of the decadal logarithm of experimentally observed and kinetic model methane yields ( $\text{mmol methane g}^{-1}$  total organic carbon (TOC) from heated New Albany Shale (NAS) versus temperature of experiments and model predictions ([Wei et al., 2018](#)).

A variety of porosimetric methods, including low pressure gas adsorption, mercury porosimetry, and small-angle neutron scattering, was used to assess macro- meso- and microporosity in shales (e.g., [Mastalerz et al., 2012](#); [Mastalerz et al., 2013](#); [Bahadur et al., 2015](#)). The results demonstrate that porosity strongly depends on the amount of organic matter and its thermal maturity. Porosity in shales at low maturity initially diminishes due to compaction, but incipient thermal cracking at the beginning of

the oil window generates new porosity. Further into the oil window, the generation of additional liquid hydrocarbons fills pores and reduces the open pore space available for gas storage until the late mature stage when secondary cracking and gas generation expels some liquid hydrocarbons and opens new pore spaces for gases. The influence of the generated hydrocarbon products on the porosity of shales was further tested, confirmed, and quantified by extracting shales with dichloromethane and toluene ([Wei et al., 2014](#)). The influence of temperature and pressure on the evolution of porosity in shales was also tested in experiments of 6 to 12 month duration and at temperatures of 60, 100, and 200 °C, and hydrostatic pressure up to 300 MPa. While small porosity differences were noted in response to temperature increase, increase in hydrostatic pressure had no measurable effect (Mastalerz et al., in review). In addition, the impact of ion milling on the maturity of shale samples with the implications for SEM analysis and SEM-documented porosity was tested on a set of shale samples of varying maturity ([Mastalerz and Schieber, 2017](#)). Our results demonstrate that more aggressive milling methods, such as the use of multiple beams and higher acceleration voltages can elevate reflectance values of organic matter and consequently can skew porosity characteristics of shale samples.

Hydrocarbon gas seepage is a significant global source of atmospheric methane, ethane and propane as greenhouse gases and photochemical pollutants. We compared the (i) regional intense natural gas seepage stemming directly from source rocks, mostly organic-rich fractured black shales in western New York State (NYS) with (ii) the areas with rare seepage in more southern regions of the Appalachian Basin and the midwestern USA ([Schimmelmann et al., in press](#)). In addition to thermogenic methane, western NYS shale gas seeps emit ethane and propane with C<sub>2+3</sub> gas concentrations reaching up to 35 vol. %. Fractures in NYS developed, reactivated and maintained permeability for gas as a result of Quaternary glaciation and post-glacial basin uplift. In contrast, more southern Appalachian and southern midwestern regions experienced less glacial loading and unloading than in NYS, resulting in less recent natural fracturing, as witnessed by the rarity of seepage on surface outcrops and in caves overlying gas-bearing shales and coals. Our survey of active gas seeps and historical literature suggests that early western NYS drilling and production of oil and gas diminished the shale gas pressure and resulted in declining gas seepage rates.

#### References:

- Bahadur, J, Radlinski, A.P., Melnichenko, Y.B, Mastalerz, M., Schimmelmann, A. (2015) Small-angle and ultrasmall-angle neutron scattering (SANS/USANS) study of New Albany Shale: A treatise on microporosity. *Energy & Fuels* 29 (2), 567-576. <http://dx.doi.org/10.1021/ef502211w>
- Mastalerz, M., He, L., Melnichenko, Y.B., Rupp, J.A. (2012) Porosity of coal and shale: Insights from gas adsorption and SANS/USANS techniques. *Energy & Fuels* 26, 5109–5120. <http://dx.doi.org/10.1021/ef300735t>
- Mastalerz, M., Schieber, J. (2017) Effect of ion milling on the perceived maturity of shale samples: Implications for organic petrography and SEM analysis. *International Journal of Coal Geology* 183, 110-119. <https://doi.org/10.1016/j.coal.2017.10.010>
- Mastalerz, M., Schimmelmann, A., Drobniak, A., Chen, Y. (2013) Porosity of Devonian and Mississippian New Albany Shale across a maturation gradient: Insights from organic petrology, gas adsorption, and mercury intrusion. *AAAP Bulletin* 97 (10), 1621–1643. <http://dx.doi.org/10.1306/04011312194>
- Mastalerz, M., Wei, L., Drobniak, A., Schimmelmann, A., Schieber, J. (in review) Responses of specific surface area and micro- and mesopore characteristics of shale and coal to heating at elevated hydrostatic and lithostatic pressures. *International Journal of Coal Geology*.

Schimmelmann, A., Ensminger, S.A., Drobniak, A., Mastalerz, M., Etiope, G., Jacobi, R.D., Frankenberg, C. (2018) Natural geological seepage of hydrocarbon gas in the Appalachian Basin and Midwest USA in relation to shale tectonic fracturing and past industrial hydrocarbon production. *Science of the Total Environment* (in press). <https://doi.org/10.1016/j.scitotenv.2018.06.374>

Wei L, Mastalerz M, Schimmelmann A, Chen Y (2014) Influence of Soxhlet-extractable bitumen and oil on porosity in thermally maturing organic-rich shales. *International Journal of Coal Geology* 132, 38-50. <http://dx.doi.org/10.1016/j.coal.2014.08.003>

Wei, L., Schimmelmann, A., Mastalerz, M., Lahann, R. W., Sauer, P.E., Drobniak, A., Strąpoc, D., Mango, F.D. (2018) Catalytic generation of methane at 60-100°C and 0.1-300 MPa from source rocks containing kerogen Types I, II, and III. *Geochimica et Cosmochimica Acta* 231, 88-116. <https://doi.org/10.1016/j.gca.2018.04.012>

## Distributary Channel Networks modeled through Non-linear Viscous Fingering

John B. Shaw, Wun-Tao Ke, Robert Mahon, Chris Cathcart

University of Arkansas

Distributary channel networks control the routing of sediment and the large-scale heterogeneity of the resulting deposit on deltaic coastlines. In certain cases, several coeval, interacting channels grow to produce a complex network. Through several analyses, we show that this network and its sedimentology and stratigraphy can be described using a model similar to that of the well-studied viscous fingering problem. Conceptually, the model is a channel network of uniform depth eroding into an unchanneled deposit of uniform thickness. The model applies the Laplace Equation to the water surface within an unchanneled domain with a constant water surface elevation. Distributary channels are leaky: flow departs over levees and flows to the basin through shallow inter-distributary bays as well as at channel tips. The Laplace Equation allows the water surface slope, shear stress, and sediment transport to be solved along the channel boundary and the network evolved through erosional translation of the upstream channel boundary. Further assuming very thin channels, this model predicts a bifurcation angle of  $72^\circ$ , which we have confirmed with measurement of 197 bifurcations on field deltas and 25 bifurcations in laboratory experiments (see Coffey and Shaw, 2017, *GRL*). We have recently extended this database into ancient channel mouth bifurcations from 3D seismic of Earth ( $n=89$ ) and from HiRISE imagery of Mars ( $n=37$ ). These ancient systems also have a mean bifurcation angle that is consistent with the  $72^\circ$  prediction of Laplacian Flow. The model has also been implemented in Matlab using the Boundary Element Method (see figure). The model reveals several interesting results. First, the model will produce arbitrarily small channels unless a smoothing length is included. We interpret this as a geomorphic constraint preventing channel width-to-depth ratios from becoming arbitrarily small. Second, the morphology of the emergent network is very sensitive to non-linear aspects of the shear stress-sediment transport relation. An exponent of 1.5 common in sediment transport formulae produces fewer, less-bulbous channels more characteristic of real distributary networks. A significant threshold of sediment transport (from sediment cohesion) also reduces the number of emergent channels. Third, it is necessary to reduce the upstream water surface elevation as the network grows to maintain a constant discharge. This causes network growth to drop exponentially (with an exponent of -0.65) with time. We have also completed several field studies in sync with the modeling. We have found that the sediment grain size decreases as a function of flow distance from the channel boundary, regardless of whether this boundary is along a channel margin or a channel tip. We have also tracked the extension of the 7 primary distributary channels of the Wax Lake Delta over the delta's 40 year life to observe the competition in growth rates between channel tips. In summary, a simple model of network formation resolving unchanneled flow with the Laplace equation can reveal controls on network growth and morphology, as well as sedimentology and stratigraphy, for certain distributary networks.

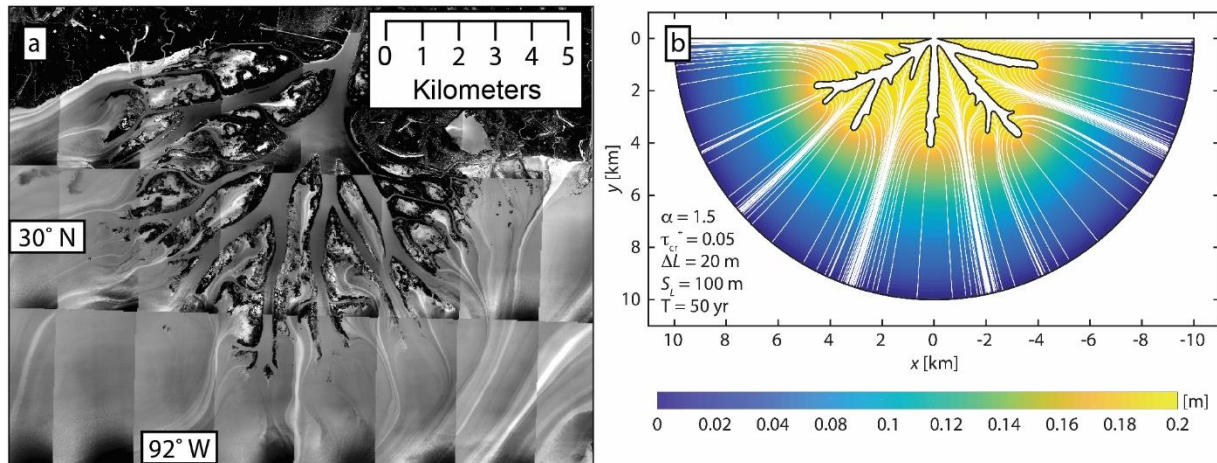


Figure 1. (a) The Wax Lake Delta in coastal Louisiana has a channel network with many channel bifurcations. The white lines on the water (on near-infrared aerial imagery) are passive tracers of flow direction. (b) A channel network generated with a moving boundary model and flow modeled with the Laplace Equation and boundary conditions similar to the Wax Lake Delta. The colormap shows the water surface elevation after 50 years of evolution. White lines are flow lines that can be compared to the flow lines in (a). Note the clustering of flow paths in the bays between the channel network in each case.

#### Most Important Publications in the Past Year

Coffey, T. S., & Shaw, J. B. (2017). Congruent Bifurcation Angles in River Delta and Tributary Channel Networks. *Geophysical Research Letters*, 2017GL074873. <https://doi.org/10.1002/2017GL074873>

Shaw, J. B., Miller, K. and McElroy, B. (2018). Island Formation Resulting from Radially Symmetric Flow Expansion, *J. Geophys. Res. Earth Surf.*, 2017JF004464, doi:10.1002/2017JF004464.

## **COUPLED ASSESSMENT OF SEISMIC, HYDRAULIC AND FRICTIONAL PROPERTIES OF FRACTURED ROCK TO ILLUMINATE FUNDAMENTAL PROCESSES GOVERNING ENERGY PRODUCTION AND WASTE STORAGE**

Parisa Shokouhi<sup>1</sup>, Jacques Rivière<sup>1</sup>, Derek Elsworth<sup>2</sup> and Chris Marone<sup>3</sup>

<sup>1</sup> Engineering Science and Mechanics, <sup>2</sup>Dept. of Energy and Mineral Engineering and Energy Institute, <sup>3</sup>Dept. of Geosciences, The Pennsylvania State University

The ultimate goal of this project is to illuminate the fundamental processes that impact fluid permeability, local seismicity rates, and earthquake triggering during drilling and fluid injection. A series of laboratory experiments are carried out to simulate changes in the local effective stress field and to simultaneously study the evolution of permeability and elasticity in relation to fracture microstructural features. We subject L-shaped samples (Westerly Granite and Green River Shale) to true tri-axial stresses of 10-50 MPa and create shear fractures in-situ while monitoring sample permeability and elastic properties. Deionized water is forced along the eventual fracture path via a differential pore pressure. Changes in the local effective stress field are imposed through normal stress or pore water pressure oscillations, with amplitudes up to a few MPa at frequencies ranging from 0.1 to 40 Hz. A multi-channel, ultrafast data acquisition system together with a set of 21 ultrasonic transducers are used to record ultrasonic data in both active and passive (acoustic emission) modes. Active ultrasonic data measured during transmission are used to obtain changes in ultrasonic wave velocity (time of flight) and attenuation (change in amplitude) before, during and after oscillations. This information is used to infer the nonlinearity of the fracture stiffness i.e., its dependence on the amplitude of the effective stress oscillations. We also monitor the evolution of permeability before and after dynamic oscillations of the fracture's effective normal stress. The fracture is subsequently sheared in two steps. During fracturing and shearing, the seismicity along the fracture is monitored passively in the acoustic emission mode. Finally, high-resolution laser profilometry is conducted on the post-mortem samples in order to reconstruct fracture aperture distribution.

The coupled assessment of ultrasonic and hydraulic data provides physical insights into how nonlinearity and permeability of the fractured interface are interrelated through fracture microscopic roughness and aperture. Our results to date indicate that nonlinearity of fractures in both Westerly Granite and Green River Shale scale with the oscillation amplitude, while shearing of the fracture reduces the nonlinearity measured during normal stress oscillations. Generally, greater permeability enhancement is observed at higher oscillation amplitudes and is more pronounced for oscillations in pore water pressure than for applied normal stress. Finally, both mechanical nonlinearity and permeability exhibit strong frequency dependencies. While the nonlinearity decreases with the frequency of normal stress oscillations, the optimal permeability enhancement for 1-MPa oscillations is achieved at 10 Hz.

A second series of experiments is conducted on pre-fractured samples of known initial fracture interface roughness. A test protocol similar to that described above is followed. High-resolution laser profilometry provides the post-shear roughness. These data provide groundtruth for interpreting the complex evolution of ultrasonic properties and permeability in samples where rough, natural fractures are produced in-situ.

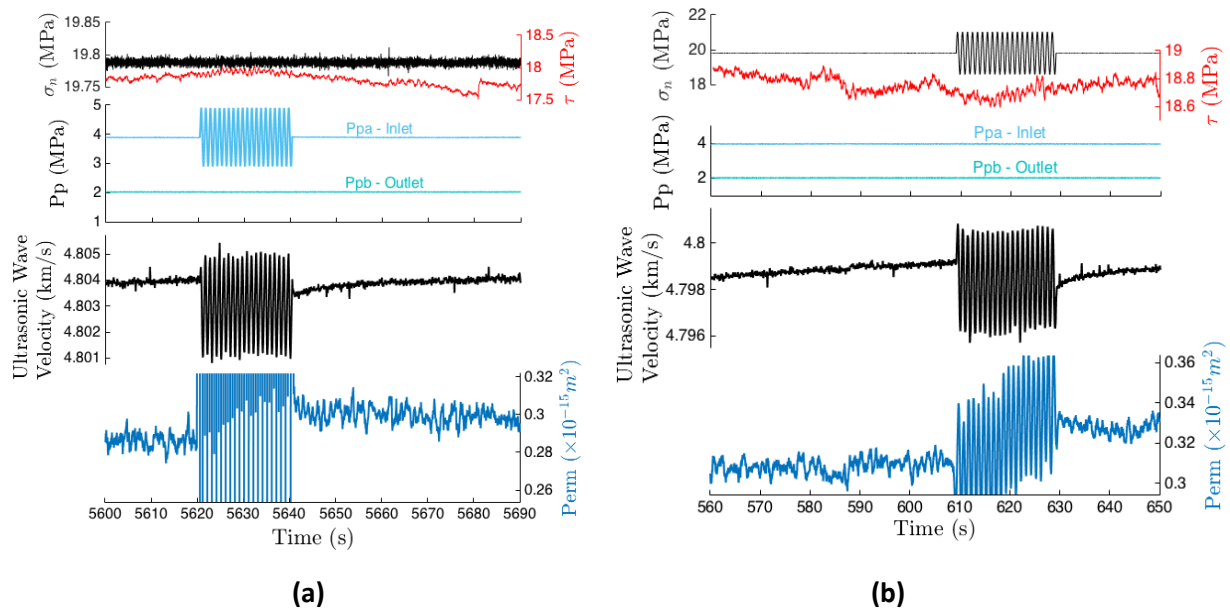


**Figure 1.** A sample data set showing changes in nonlinearity and permeability due to oscillations in (a) pore water pressure and (b) normal stress. The top plot in each figure shows the normal stress and shear stress variations over time. The second plot from the top illustrates how the pore water pressures in inlet (Ppa) and outlet (Ppb) evolve. The bottom two plots give the changes in ultrasonic wave velocity and permeability. The nonlinearity manifests itself through the initial drop and fluctuations of ultrasonic wave velocity during effective stress perturbation as well as slow post-oscillation recovery. The permeability enhancement is quantified in terms of the relative change in permeability due to effective stress oscillations.

## OUTCOME TO DATE

1. Shokouhi, P., Rivière, J., Guyer, R. A., & Johnson, P. A. (2017) Slow Dynamics of Consolidated Granular Systems: Multi-scale Relaxation. *Applied Physics Letters*, 111, 251604.
2. Jin, J., Rivière, J., Ohara, Y., & Shokouhi, P. (2018) Dynamic Acousto-Elastic Response of Single Fatigue Cracks with Different Microstructural Features: An Experimental Investigation. *Journal of Applied Physics* [in press].
3. Shokouhi, P., Madara, B., Wood, C., Rivière, J., Elsworth, D., Marone, C. & Johnson, P. A. Coupled Assessment of Seismic, Hydraulic and Frictional Properties of Fractured Rock. *Penn State Energy Days*, University Park, PA, May 30, 2018. [abstract and poster presentation]
4. Shokouhi, P., Madara, B., Wood, C., Rivière, J., Elsworth, D., & Marone, C. Elastic Nonlinearity of Fractured Rocks and Its Relation to Fluid Permeability. *ISNA/ICNEM*, Santa Fe, NM, July 12, 2018. [abstract and conference presentation]
5. Madara, B., Rivière, J. and C. Marone, Permeability Evolution as a Function of Fracture, Shear, and Dynamic Stressing Under True Triaxial Load, Submitted to *Geochem., Geophys., and Geosystems*, 2018.

## Mineral precipitation in porous media: interplay between transport, nucleation and growth

V. Starchenko, M. C. Cheshire, J. Weber, A. G. Stack

Understanding reactions in porous materials impacts a wide range of energy-related applications including CO<sub>2</sub> sequestration, oil and gas extraction, design of energy storage systems (e.g. batteries and supercapacitors), and supported catalysts. Heterogeneous mineral precipitation in porous media is a complex phenomenon which includes an interplay between transport of the reactant into the matrix, crystal nucleation on the surface, and crystal growth processes. Barite (BaSO<sub>4</sub>) is considered a potential material for contaminant confinement during hydraulic fracturing due to its ability to incorporate radium and strontium ions into the crystal lattice.

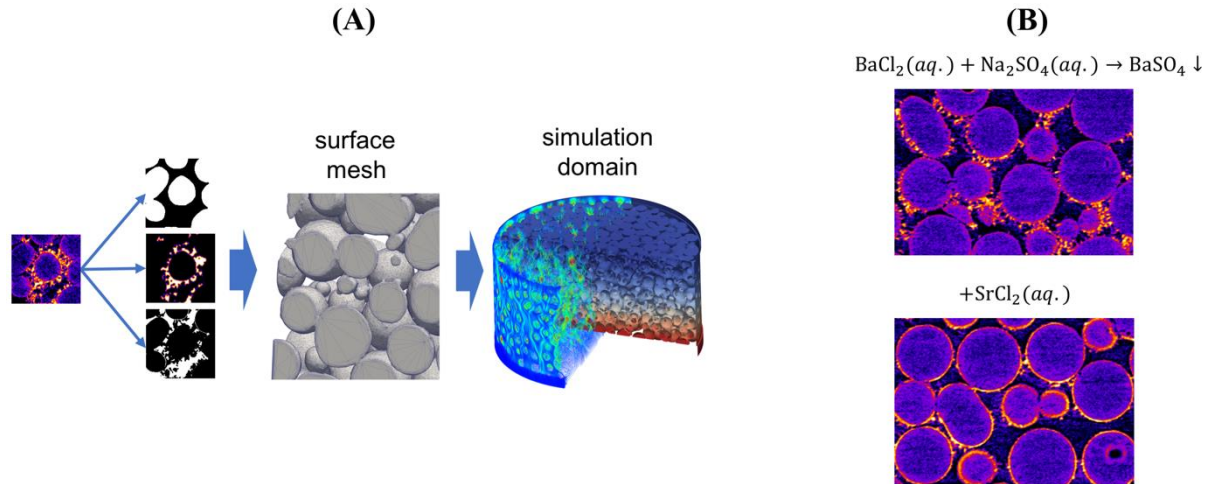


Figure 1. (A) Schematic path from tomography experiment to simulations used in this study to explain barite precipitation. (B) Tomography images of barite precipitate on the surface of glass beads without and with addition of strontium.

Our previous studies of barite crystal growth on glass surfaces have shown growth rates of individual crystal faces respond nonproportionally to solutions of different saturation index, ionic strength, and strontium impurity ions. Recent synchrotron X-Ray tomography experiments on barite precipitation within porous systems (packed beds of glass spheres) have shown that barite morphology depends on the flow rate and impurities present. Figure 1 (A) schematically shows a sequence of postprocessing steps we typically need to convert the tomography images into the simulation domain for pore scale modelling. While conventional methods like thresholding or watershed failed to produce clean segmentation, better results have been achieved by using segmentation powered by machine learning algorithms. Figure 1 (B) shows the tomography images of barite precipitation on the surface of glass beads after 6 hours experiment without (top) and with addition of Sr<sup>2+</sup> (bottom) to the system. Different barite morphology (it becomes more compact and uniform around the particles) in presence of strontium indicates the shift in crystal growth – crystal nucleation balance towards a nucleation dominant process. Consequently, understanding how to tune the balance between nucleation and growth processes by chemistry of reactive flow will allow us to regulate the porosity/permeability relation and its evolution in time.

## **Shales and geological waste repositories: from microstructure description to macro-scale properties**

Christophe Tournassat<sup>1,2,3</sup>, Stéphane Gaboreau<sup>2</sup>, Carl I. Steefel<sup>1,1</sup> Energy Geoscience Division, Lawrence Berkeley National Laboratory, Berkeley, CA 94720, USA <sup>2</sup>BRGM, Orléans, 45060, France <sup>3</sup>Univ. Orléans, UMR 7327 CNRS-BRGM-ISTO, 45071 Orléans, France

Clay materials, including shales, have been the subject of longstanding study for their potential roles in the long-term disposal of nuclear wastes in geological repositories. The low permeability and hydraulic conductivity, high adsorption capacity and swelling behavior of clays provide numerous functions for the confinement of radionuclide contaminants. These desirable macroscopic properties are governed by mineralogical properties and chemical processes that are not understood at a fundamental level. In particular, the negative electrostatic charge of clay minerals exerts a dominant influence on the aqueous chemistry of water-saturated nanoscale pores and interlayers as well as a remarkable array of macroscale properties. In this presentation we will highlight the complex interplays of mineralogical, chemical and microstructural characteristics of clay materials that lead to high osmotic and crystalline swelling pressure, semi-permeable membrane properties, and non-Fickian diffusional behavior.

Numerical methods for modeling macroscopic properties of nanoporous charged media are of growing interest to diverse research communities. A coupled reactive modeling approach at the continuum scale, which can handle the consideration of overlapping diffuse layers at the nanoscale, will be described. In addition, the presentation will review the many theoretical and numerical challenges that must be overcome to mechanistically simulate transient chemo-mechanic regimes in clay samples exposed to changing in chemical conditions.

## In situ Microanalysis of O & C Isotope Ratios in Carbonate Cements: Calcite Revisited

John W. Valley, University of Wisconsin-Madison

### PROJECT OBJECTIVES (DE-FG02-93ER14389)

- Improve microanalytical techniques for *in situ* analysis of O and C isotope ratios by SIMS (ion microprobe). Develop SIMS standards for oxygen and carbon isotope analysis of carbonates at sub-1 to 10-micron scale.
- Apply new SIMS techniques in studies including: biogenic carbonates, carbonates associated with serpentinization, and diagenetic, hydrothermal and pedogenic carbonate cements in sedimentary rocks.
- Determine: the presence, abundance, relative timing and chemo-isotope composition of different generations of porosity-reducing carbonate cements in the Bakken Formation, ND.

Better understanding of genesis and timing of carbonate precipitation contributes to larger DOE objectives, including: CO<sub>2</sub> sequestration in sedimentary basins; interpreting proxies of paleoclimate; subsurface fluid flow; water/rock interaction; and characterizing properties of oil, gas, and potable water reservoirs.

Highly precise, *in situ* analysis of stable isotope ratios is possible from 1-10 μm spots with large radius multi-collector SIMS instruments such as the IMS-1280. Accuracy, however, requires calibration standards that are chemically and crystallographically matched to samples. In the past, all calcite has been calibrated against a single standard and other carbonates have been calibrated against linear interpolations of end-member standards. We have identified homogeneous natural carbonates by analyzing ~150 samples and calibrated 28 Ca-Mg-Fe-Mn compositions (Fig. 1b; Sliwinski et al. 2017a, Kitajima et al. unpd). Instrumental bias is surprisingly non-linear and minor element variability in calcite must be considered. Accurate analysis (±0.5‰) requires full characterization of minor elements. Young biocarbonates present a special problem and show systematic differences in SIMS bias (IMF) that correlate to [OH] (simultaneously measured by SIMS, Fig. 1a; Orland et al. 2015, Linzmeier et al. 2018, Helser et al. 2018, Wycech et al. 2018, Ishida et al. 2018), although this offset has not been observed in carbonates older than 40 ka. Understanding the cause and making accurate corrections in biocarbonates will require more complete characterization of the hydrous component(s).

Detailed patterns of growth zoning and diagenesis have been interrogated using the new carbonate SIMS standards including:

GSMS and SIMS analyses of δ<sup>18</sup>O were compared in **fish otoliths** (Helser et al. 2018). The fractionation of δ<sup>18</sup>O in embryonic cores of otoliths was calibrated for Japanese glass eels grown in captivity and applied to wild-caught eels; water temperature and thus depth of the spawning area is shown to be upper-most part of the thermocline (Shirai et al. 2018).

Comparison of embryonic vs. post-hatching shells show that **ammonite** eggs were benthic and that hatchlings migrated to shallower water in the Upper Cretaceous Fox Hills Fm (Linzmeier et al. 2018).

Studies of **foraminifera** calibrate the GSMS-SIMS offset for δ<sup>18</sup>O (Wycech et al. 2018) and show that when altered domains are excluded the marine carbon isotope excursion for “hot-house” environments at the Paleocene-Eocene Thermal Maximum (PETM) is 2‰ larger than in whole-shell studies, in-line with the terrestrial record (Kozdon et al. 2018).

The Devonian/Mississippian **Bakken** Petroleum System in the Williston Basin includes major unconventional tight oil reservoirs. This work builds on our previous studies of diagenesis in

hydrocarbon-poor lithologies from the Illinois Basin (Denny et al. 2017, Sliwinski et al. 2017b). Early calcite cements reduce porosity in the Middle Bakken and isotopically resemble recrystallized marine carbonates. Over 8 generations of later dolomite cements vary by up to 8‰ in  $\delta^{18}\text{O}$  and sharp gradients exist in  $\delta^{13}\text{C}$  (to 9‰/100 $\mu\text{m}$ ) with values to -9‰ likely recording the onset of organic matter maturation in adjacent shale (Brodie et al. 2018, Denny et al. in prep., Sliwinski et al. in prep.). The formation of these zoned dolomite cements enhanced reservoir properties by preserving and creating porosity for storing hydrocarbons.

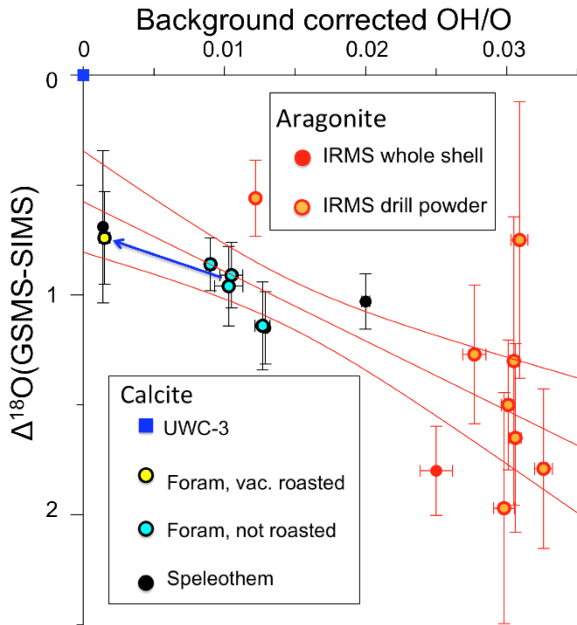


Fig. 1a

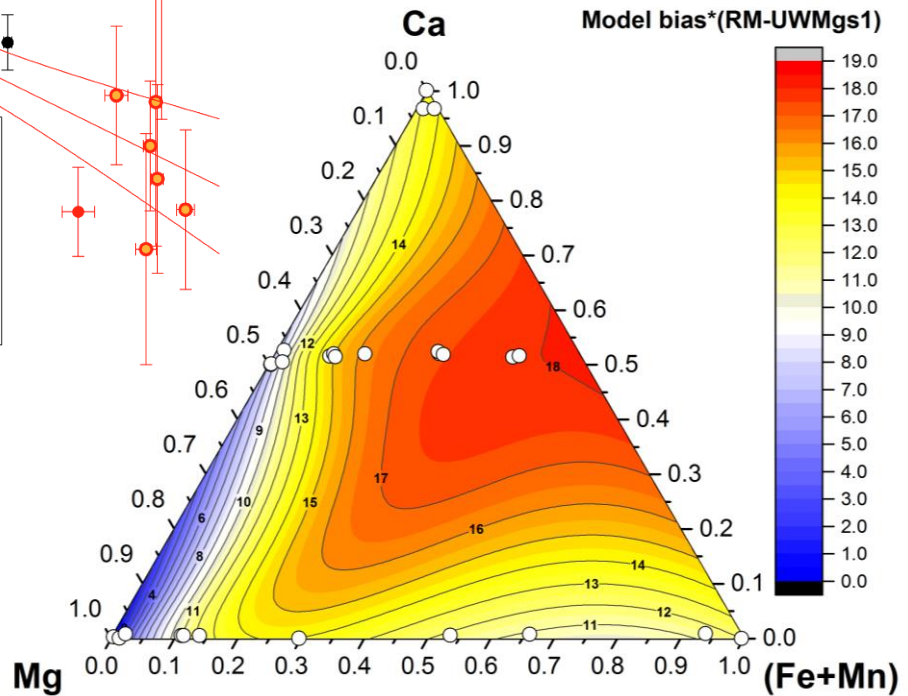


Fig. 1b



Brodie MW, Aplin AC, Hart B, Orland I, Valley JW, Boyce AJ (2018) Oxygen Isotope Microanalysis by Secondary Ion Mass Spectrometry Suggests Continuous 300 Million Year History of Calcite Cementation and Dolomitization in the Devonian Bakken Formation. *J. Sed. Res.* 88: 91-104.

Denny AC; Kozdon R; Kitajima K; Valley JW (2017) Isotopically Zoned Carbonate Cements in Early Paleozoic Sandstones of the Illinois Basin:  $\delta^{18}\text{O}$  and  $\delta^{13}\text{C}$  Records of Burial and Fluid Flow. *Sed. Geol.*, 361: 93-110.

Helser T, Kastle C, McKay J, Orland IJ, Kozdon R, Valley JW (2018) Evaluation of micromilling/conventional isotope ratio mass spectrometry and secondary ion mass spectrometry of  $\delta^{18}\text{O}$  in fish otoliths for sclerochronology. *Rapid Comm. in Mass Spectrometry*. Accepted May 2018

Ishida A, Kitajima K, Williford KH, Kakegawa T, Valley JW (2018) Simultaneous in situ analysis of carbon and nitrogen isotope ratios in the organic matter by secondary ion mass spectrometry. *Geostandards and Geoanalytical Research*, v. 42, #2, DOI: 10.1111/ggr.12209

Kozdon R, Kelly DC, Valley JW (2018) Diagenetic Attenuation of Carbon Isotope Excursion Recorded by Planktic Foraminifers during the Paleocene-Eocene Thermal Maximum. *Paleocean. & Paleoclim.*, 33: 367-380.

Linzmeier BJ, Landman NH, Peters SE, R Kozdon R, Kitajima K, Valley JW (2018) Ion microprobe stable isotope evidence for ammonite habitat and life mode during early ontogeny. *Paleobiology*. DOI: 10.1017/pab.2018.21.

Shirai K, Otake T, Amano Y, Kuroki M, Ushikubo T, Kita NT, Murayama M, Tsukamoto K, Valley JW (2018) Temperature and depth distribution of Japanese eel eggs estimated using otolith oxygen stable isotopes. *Geochim Cosmochim Acta*. doi.org/10.1016/j.gca.2018.03.006.

Śliwiński MG, Kitajima K, Kozdon R, Spicuzza MJ, Denny A and Valley JW (2017a) In situ  $\delta^{13}\text{C}$  and  $\delta^{18}\text{O}$  microanalysis by SIMS: A method for characterizing the carbonate components of natural and engineered  $\text{CO}_2$ -reservoirs. *International Journal of Greenhouse Gas Control*, 57: 116-133.

Śliwiński MG, Kitajima K, Spicuzza MJ, Orland IJ, Ishida A, Fournelle JH, Valley JW (2017b) SIMS bias on isotope ratios in Ca-Mg-Fe carbonates (Part III):  $\delta^{18}\text{O}$  and  $\delta^{13}\text{C}$  matrix effects along the magnesite-siderite solid-solution series. *Geostandards and Geoanalytical Research*. 42: 49-76.

Wycech J, Kelly DC, Kozdon R, Orland I, Spero HJ, Valley JW (2018) Comparison of  $\delta^{18}\text{O}$  Analyses on Individual Planktic Foraminifer (*Orbulina universa*) Shells by SIMS and Gas-Source Mass Spectrometry. *Chem. Geol.* 483:119-130.

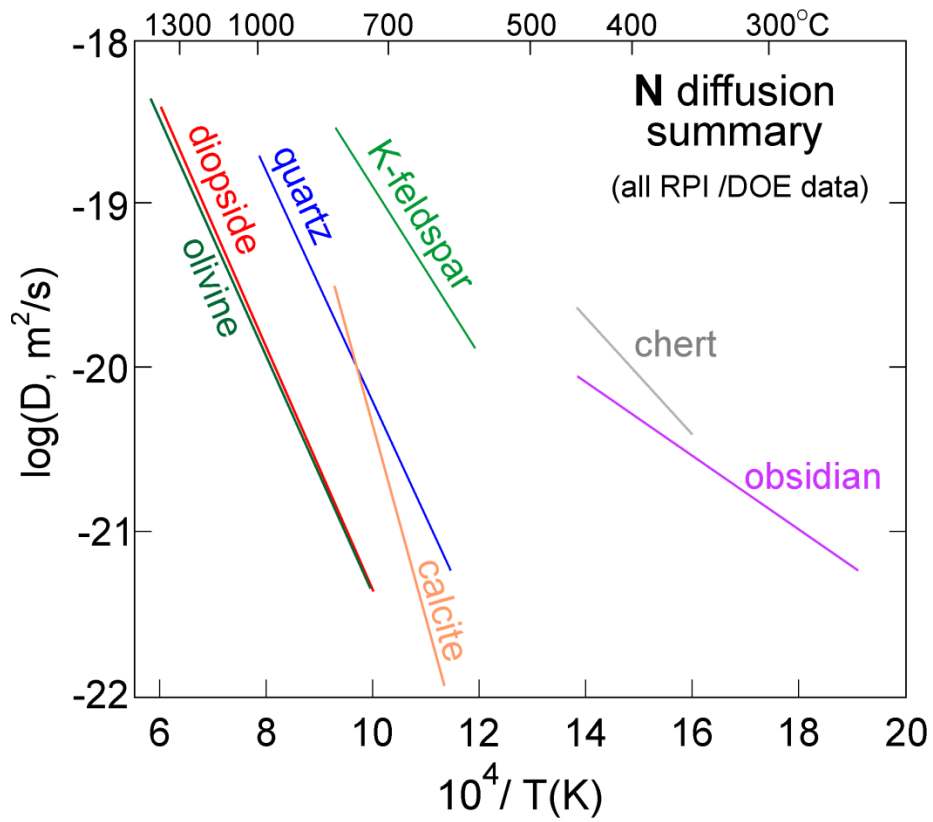
## Nitrogen diffusion in minerals, with implications for terrestrial N cycling

E. Bruce Watson<sup>1</sup>, Daniele J. Cherniak<sup>1</sup>, Morgan F. Schaller<sup>1</sup>, Richard L. Hervig<sup>2</sup> <sup>1</sup> Department of Earth & Environmental Sciences, Rensselaer Polytechnic Institute <sup>2</sup> School of Earth & Space Exploration, Arizona State University

Despite the geochemical importance of nitrogen, the behavior of this element in the solid Earth is poorly constrained, particularly in terms of interactions with major rock-forming minerals. An understanding of N diffusion in these materials is a potentially important part of the overall picture. To this end, we have obtained well-constrained diffusion laws for nitrogen in quartz, K-feldspar, clinopyroxene, olivine and calcite using nuclear reaction analysis (NRA) to depth-profile <sup>15</sup>N diffused into mineral specimens from a C-H-O-N vapor/fluid source and/or introduced by ion implantation and mobilized by annealing. The "global" temperature range of our data set is ~500-1400°C but is more restricted for individual minerals due to their differing thermal stabilities. Most experiments were conducted at near-atmospheric pressure, complemented by some runs at 1 GPa. Time series were included in our protocols for all 5 minerals, generally spanning nearly a factor of 10 in duration. Depth profiling of in-diffusion and ion-implantation experiments by NRA yields highly consistent results. In addition, two experiments were profiled by SIMS as well as by NRA, also with consistent results. The activation energies for N diffusion are similar for olivine, diopside and quartz (~140 kJ/mol), highest for calcite (~230 kJ/mol) and lowest for orthoclase (~100 kJ/mol). Diffusivities at 1 GPa are statistically indistinguishable from those acquired at low pressure. Arrhenius laws for N diffusion generally differ markedly among the 5 minerals investigated, except for those of olivine and clinopyroxene, which are nearly identical. At ~600°C,  $D_N$  ranges from  $2.3 \times 10^{-20}$  m<sup>2</sup>/s for orthoclase to  $3.9 \times 10^{-23}$  m<sup>2</sup>/s for olivine and clinopyroxene.

Compared with noble-gas diffusion behavior reported in the literature, N diffusion in most minerals is quite slow. Some broad (and preliminary) implications are as follows: 1) N released to the mantle wedge from subducted assemblages equilibrates locally with pyroxene and olivine grains on relatively long times scales of 10<sup>6</sup> to 10<sup>8</sup> years; 2) "biological" N ultimately captured in high-grade metamorphic minerals is released very slowly on the retrograde limb of a metamorphic cycle (which makes it available to biology during denudation); and 3) diffusive exchange of N captured in fluid inclusions in calcite (or in the calcite lattice) is essentially nonexistent over geologic time.

Although our work has not been aimed specifically at N solubility in minerals and fluid/mineral partitioning, our in-diffusion experiments provide some insight into N uptake from C-H-O-N vapor or fluid. In the experiments at near-atmospheric pressure, N concentrations range from ~30-50 ppm in quartz, ~60-250 ppm in olivine, and ~100-2600 ppm in orthoclase.



## Atomic Structure, Defects, and Stacking of Clay Particles by Low-Dose, High Resolution (Cryo)-TEM

Michael L. Whittaker<sup>1,2</sup>, Christian Kisielowski<sup>3</sup>, Colin Ophus<sup>3</sup>, Benjamin Gilbert<sup>1</sup>, and Jillian F. Banfield<sup>1,2</sup><sup>1</sup>. Energy Geoscience Division, Lawrence Berkeley National Laboratory, Berkeley CA <sup>2</sup>. Department of Earth and Planetary Science, University of California Berkeley, Berkeley CA <sup>3</sup>. National Center for Electron Microscopy, Lawrence Berkeley National Laboratory, Berkeley CA

Clay minerals play important roles in myriad natural phenomena and engineered systems, from earthquakes and mudslides to barriers for nuclear waste storage and caprocks for anthropogenic carbon sequestration. Swelling clays are especially important, with chemical-mechanical behavior that arises from the competing forces between hydrated and charged layers 1 nm thick and up to a few microns wide. Our ability to predict the expansion or collapse of swelling clays in response to changing environmental conditions is limited by incomplete knowledge of the structures of clay layers, including substitutions and defects, and the interactions between them. These control the mechanisms through which the layers stack or disassemble and the larger-scale structure of clay particles. Here, we present new high-resolution observations of clay layer structure and mechanistic studies of expansion and collapse under rapid changes in aqueous chemistry.

Unprecedentedly high resolution images of single layers of montmorillonite were obtained using low-dose high-resolution transmission electron microscopy (HRTEM). Electron-beam induced damage, the prevailing limitation to high-resolution imaging of clays for over 3 decades, was found to be minimized at low total dose but, counterintuitively, high dose rate. We attribute this behavior to hydrolysis of interlayer water and the subsequent damage cascade from charged byproducts. At total electron doses less than  $\sim 500 \text{ e}^-/\text{\AA}^2$ , a maximum resolution of 1  $\text{\AA}$  along the [001] zone axis was achieved. Single-layer images revealed the existence of strain with few-nanometer length scale clearly associated with local defect disorder. Edge structures were also clearly resolved, showing far more disorder than typically modeled.

Dynamic interactions within stacks of clay layers in aqueous solution were investigated by time-resolved small-, medium- and wide-angle synchrotron X-ray scattering, and corroborated with low-dose cryo-TEM. The exchange of potassium for sodium in the interlayer space was found to occur within seconds, accompanied by transition of the interlayer hydration state from three to two discrete layers of water. However, theory predicts that complete cation exchange should occur within milliseconds. Using cryo-TEM, we directly measure the average interlayer separation and see evidence for rotational interparticle ordering that is dependent on the cation concentration and type and may represent the rate limiting step in the process of collapse.

## Divalent Mn-Promoted Rapid Transformation of Layered to Tunneled Manganese Oxide

Mengqiang Zhu<sup>1</sup>, Peng Yang<sup>1</sup>, Seungyeol Lee<sup>2</sup>, Jeffrey E. Post<sup>3</sup>, Huifang Xu<sup>2</sup>, Qian Wang<sup>1</sup>, and Wenqian Xu<sup>4</sup>  
<sup>1</sup> Department of Ecosystem Science and Management, University of Wyoming, Laramie, WY 82071  
<sup>2</sup> Department of Geoscience, University of Wisconsin-Madison, Madison, WI 53706  
<sup>3</sup> Department of Mineral Sciences, Smithsonian Institute, Washington, DC 20013  
<sup>4</sup> X-ray Science Division, Advanced Photon Source, Argonne National Laboratory, Argonne, IL 60439

**Abstract:** Tunneled manganese (Mn) oxides (TMOs), with both environmental and economic significance, form from topotactic transformation of layered manganese oxides (LMOs), but the transformation is deemed to be very slow at room temperature, and laboratory syntheses require elevated temperature. This study explores the possibility for LMOs transform to TMOs at room temperature and environmentally relevant pHs. Divalent Mn (Mn(II)) pre-loaded  $\delta$ -MnO<sub>2</sub> (Mn(II)-MnO<sub>2</sub>) was incubated in 100 mM NaCl solution at 21 °C and pH 6 – 8 for 25 days. The incubation resulted in rapid transformation of Mn(II)-MnO<sub>2</sub> to a 4 × 4 TMO. The rapid transformation was triggered by the presence of a high amount of vacancy-adsorbed Mn(III) due to the comproportionation between the vacancy-adsorbed Mn(II) and Mn(IV) in  $\delta$ -MnO<sub>2</sub>. The transformation was fastest at pH 7 but slower at pH 6 or 8 due to an insufficient produced Mn(III) (pH 6) or formation of a less viable precursor (triclinic birnessite) (pH 8). The presence of O<sub>2</sub> favors the formation of triclinic birnessite at pH 8 and thus retards the transformation, whereas it enhances production of vacancy-adsorbed Mn(III) at pH 6 and 7 and promotes the transformation. Co-existing cations strongly affected the LMO-to-TMO transformation. Monovalent cations (Li<sup>+</sup>, Na<sup>+</sup> and K<sup>+</sup>) promoted the transformation while both Ca<sup>2+</sup> and Mg<sup>2+</sup> led to formation of triclinic birnessite and thus inhibited the transformation. For Cu<sup>2+</sup>, it also inhibits the transformation but via preventing Mn(III) formation in  $\delta$ -MnO<sub>2</sub> structure. Our work discovers the role of Mn(III) in the layered-to-tunneled structural transformation, and suggests that TMOs can form from LMOs in the low-temperature environment much faster than previously assumed. The relative low abundance of TMOs compared to LMOs in natural environment might be caused by impurity cations (such as transition metals) in the structure of LMOs.